AD-A132 084 PSEUDOSPECTRAL SOLUTION OF INVISCID FLOWS WITH MULTIPLE DISCONTINUITIES(U) NAVAL RESEARCH LAB WASHINGTON DC L SAKELL 17 AUG 83 NRL-MR-5147 1/1

UNCLASSIFIED F/G 20/4 NL

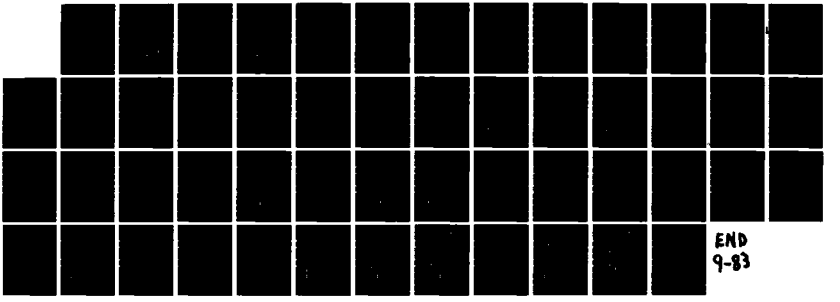

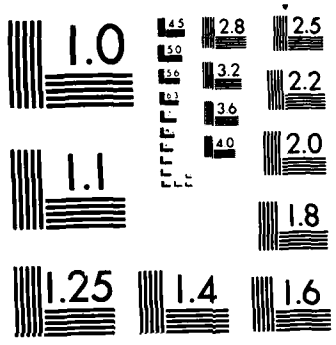

(2)

NRL Memorandum Report 5147

Pseudospectral Solution of Inviscid Flows with Multiple Discontinuities

L. SAKELL

Fluid Dynamics Branch
Marine Technology Division

August 17, 1983

NAVAL RESEARCH LABORATORY
Washington, D.C.

SECURITY CLASSIFICATION OF THIS PAGE (When Data Entered)

REPORT DOCUMENTATION PAGE		READ INSTRUCTIONS BEFORE COMPLETING FORM
1. REPORT NUMBER NRL Memorandom Report 5147	2. GOVT ACCESSION NO.	3. RECIPIENT'S CATALOG NUMBER
4. TITLE (and Subtitle) PSEUDOSPECTRAL SOLUTION OF INVISCID FLOWS WITH MULTIPLE DISCONTINUITIES		5. TYPE OF REPORT & PERIOD COVERED Interim report on a continuing NRL problem. 6. PERFORMING ORG. REPORT NUMBER
7. AUTHOR(s) L. Sakell		8. CONTRACT OR GRANT NUMBER(s)
9. PERFORMING ORGANIZATION NAME AND ADDRESS Naval Research Laboratory Washington, DC 20375		10. PROGRAM ELEMENT, PROJECT, TASK AREA & WORK UNIT NUMBERS 61153N; RR021-05-4B; 58-1839-03
11. CONTROLLING OFFICE NAME AND ADDRESS		12. REPORT DATE August 17, 1983 13. NUMBER OF PAGES 51
14. MONITORING AGENCY NAME & ADDRESS(if different from Controlling Office)		15. SECURITY CLASS. (of this report) UNCLASSIFIED 15a. DECLASSIFICATION/DOWNGRADING SCHEDULE

16. DISTRIBUTION STATEMENT (of this Report)

Approved for public release; distribution unlimited.

17. DISTRIBUTION STATEMENT (of the abstract entered in Block 20, if different from Report)

18. SUPPLEMENTARY NOTES

19. KEY WORDS (Continue on reverse side if necessary and identify by block number)

Pseudospectral	Euler equations	Inviscid flow
Chebyshev	Artificial viscosity	Bursting diaphragm
Colliding shock waves		

20. ABSTRACT (Continue on reverse side if necessary and identify by block number)

Pseudospectral techniques are used to compute two time dependent flows: bursting diaphragm flow and the flow created when two normal shock waves collide. Solutions are obtained by integrating the time dependent Euler equations of motion cast in conservation law form.

DD FORM 1 JAN 73 1473 EDITION OF 1 NOV 65 IS OBSOLETE
S/N 0102-014-6601

SECURITY CLASSIFICATION OF THIS PAGE (When Data Entered)

CONTENTS

PSEUDOSPECTRAL SOLUTION OF INVISCID FLOWS WITH MULTIPLE DISCONTINUITIES

I. INTRODUCTION

The author has shown [1-3] that a pseudospectral technique may be coupled with fourth-order artifical viscosity and spectral filtering [4] to solve inviscid flow fields in which a single discontinuity is present. The flow fields treated in this manner have been both one and two dimensional in character; the former consisting of a shock wave propagating in the co-ordinate direction and the latter a supersonic wedge flow. This report presents results using that same combination of smoothing techniques applied to flows where multiple discontinuities arise. As in Reference 1, the full inviscid equations of motion (Euler equations), cast in conservation law form, are used together with an Adams-Bashforth time differencing algorithm.

Two classes of multiple discontinuity inviscid flows are solved: (1) a bursting diaphragm problem, in which a shock wave and contact surface discontinuity are simultaneously present, but neither have yet reached a boundary, and (2) the flowfield which arises when two normal shock waves of unequal strengths, traveling towards each other, collide and give rise to two shock waves of new and different strengths along with a contact surface discontinuity.

II. Solution Technique

The time-dependent, one-dimensional, Euler equations of motion in conservation form are given by:

$$\frac{\partial \vec{U}}{\partial t} + \frac{\partial \vec{E}}{\partial x} = 0, \qquad (1a)$$

Manuscript approved June 8, 1983.

where

$$\vec{U} = \begin{bmatrix} \rho \\ \rho u \\ e \end{bmatrix}, \qquad \vec{E} = \begin{bmatrix} \rho u \\ \rho + \rho u^2 \\ (e+p)u \end{bmatrix},$$

$$e = \frac{p}{\gamma - 1} + \frac{1}{2}\rho \, [u^2]. \tag{1b}$$

and p is the pressure, ρ the density, u the velocity, and e the energy. Equation (1a) is solved in the following manner. The spatial derivative is obtained pseudospectrally. Starting with known values of the vector elements of $\vec{E}$ at a specified time, a Chebyshev series is fitted to the values of each $\vec{E}$ element. The Chebyshev series is represented by

$$E(x,t) = \sum_{n=0}^{N} A_n(t) T_n(x), \tag{2}$$

where the Chebyshev functions, $T_n(x)$, are defined by

$$T_n(x) = \cos \left[n \cos^{-1} (x) \right]. \tag{3}$$

The collocation points where the numerical values of $\vec{E}$ are known are given by

$$x_j = \cos \frac{\pi j}{N}, \qquad 0 \leq j \leq N. \tag{4}$$

Therefore, equation (2) becomes

$$E(x_j,t) = \sum_{n=0}^{N} A_n(t) \cos \frac{\pi j n}{N}. \tag{5}$$

To fit a Chebyshev series to the $\vec{E}$ data requires the solution of (5) for the A_n's. This is done using an inverse FFT.

The spatial derivative is then determined from the A_n's in the following way. A different Chebyshev series is used to represent the spatial derivative.

$$\frac{\partial \vec{E}}{\partial x} = \sum_{n=0}^{N} A_n^{(1)}(t)\, T_n(x), \tag{6}$$

where

$$A_n^{(1)} = \frac{2}{C_n} \sum_{\substack{p=n+1 \\ p+n=\text{odd}}}^{N-1} pA_p, \tag{7}$$

$$C_0 = 2,\ C_n = 1 \text{ for } 0 < n \leq N,$$

$$A_N^{(1)} = 0.0 .$$

Performing the sum in (7) for the $A_n^{(1)}$'s and using a direct FFT in (6) yields the spatial derivative values at each of the collocation points.

The solution for $\vec{U}$ is then advanced in time by using the Adams Bashforth algorithm.

$$\vec{U}_j^{\,t+\Delta t} = \vec{U}_j^{\,t} + \frac{3}{2}\Delta t \left(\frac{\partial \vec{E}}{\partial x}\right)_j^{t} - \frac{1}{2}\Delta t \left(\frac{\partial E}{\partial x}\right)_j^{t-\Delta t} + D_j. \tag{8}$$

This process (equations 5 through 8) is then cyclically repeated. The dissipation term D_j is evaluated from the following finite difference representation of a fourth derivative.

$$D_j = -\mu \left\{U_{j+2} + U_{j-2} - 4\left[U_{j+1} + U_{j-1}\right] + 6\, U_j\right\}, \tag{9}$$

where j denotes the spatial position (collocation point) index. The spectral filter (reference 4), used to damp out the high frequency solution components, is given by

$$e^{-\alpha \left\{\frac{K_n - K_o}{K_{max} - K_o}\right\}^4}; \tag{10}$$

where K_n is the spectral wave number, K_{max} is the maximum wave number (corresponding to the total number of collocation points) and $K_o \approx \frac{5}{6} K_{max}$.

The time integration step size was determined from the pseudospectral form of the Courant-Fredrich-Lewy (CFL) condition, with a Courant number of 0.5.

$$\Delta t \leq \frac{8.0\ CN}{N^2\ \max\ (|u|+c)} \qquad (11)$$

Here u is the velocity, N is the total number of points, c is the speed of sound, and CN is the Courant number.

The boundary conditions were based on the flow which arose at each boundary. For the bursting diaphragm problem, there was no flow (velocity = zero) at the boundaries. (The calculations were terminated before the shock or expansion fan reached a boundary.) Therefore, the boundary conditions were to keep all physical variables held fixed throughout the computation. For the colliding shock waves problem, variables were held fixed at supersonic inflow boundaries. This is a physical boundary condition since the integration times were kept well below those where either the contact surface or shock wave reached their respective boundaries. Outflow boundary conditions, namely the derivative equal to zero, were not considered in the present work. However, at subsonic inflow boundaries, a different approach was used. At a subsonic inflow boundary two inflow characteristics exist, namely $\frac{dx}{dt} = u$ and $u + c$. The single outgoing characteristic propagates along $\frac{dx}{dt} = u-c$. The respective characteristic values are $(p - \rho c^2)$, $(p + \rho uc)$ and $(p - \rho uc)$, where c is the speed of sound. Following reference 5 two flow variables are specified at the subsonic inflow boundary, and the third is computed from the calculated value of the outgoing characteristic.

III. BURSTING DIAPHRAGM RESULTS

Two cases were considered:

	Pressure Ratio	Density Ratio
(1)	5 to 1	2 to 1
(2)	10 to 1	8 to 1

They will be discussed sequentially.

Results for case (1) are shown in figures 1 through 4. The diaphragm separating the two stagnation zones is located at x = 0.0. One hundred twenty-eight Chebyshev series terms were used to represent the flow. The time integration was carried out to t = 0.378 (3500 time steps). The analytic solution is represented by the solid line. The dashed line represents the analytic position of the contact surface discontinuity. The angled solid line represents the expansion fan. At all times the shock wave is correctly represented as a discontinuity traveling with the proper velocity (no phase error). The contact discontinuity is spread uniformly over four to five grid points. That is, the points all fall on a straight line whose slope is slightly less than ninety degrees (the exact discontinuity value). The same behavior is present in the energy plots. It is not as clearly visible in the figures because the difference in energies on the two sides of the contact surface front are very small in comparison to the difference in densities. The pressure and velocity correctly show no variation across the contact front. The expansion fan is represented properly. Some minor humps are present both on the high and low state variable sides, and there is a slight mismatch in slope. This mismatch is a function of the physical variable being plotted. It is greatest for the velocity while least (and about the same) for the remaining three flow variables.

Results for case 2 are shown in figures 5 through 8. The attributes discussed above are also present here, as is expected. In the velocity plots there are two zones of oscillations in the region behind the shock wave. It turns out that the dividing line is the contact surface location. In front of the contact surface these oscillations are very small, while behind it they are non-existent. Additional dissipation would remove this imperfection but at the expense of a minor loss of shock resolution.

IV. COLLIDING SHOCK WAVES PROBLEM

To the authors's knowledge this is the first time this problem has been treated by pseudospectral means. Two cases are considered:

	Left Hand Side Shock	Right Hand Side Shock
(1)	M = 2.5	M = 1.5
(2)	4.0	1.5

The right hand side shock wave is propagating to the left while the left hand side shock wave propagates to the right. These two cases were chosen because after the shock waves intersect, the shock on the left (initially on the right) moves in different directions with respect to ground fixed coordinates for each case. It moves to the left for case 1 and to the right for case 2. These cases result in supersonic inflow at the left hand side computational boundary and subsonic inflow at the right hand side computational boundary. The boundary conditions were to keep all flow variables fixed at supersonic inflow points, while at subsonic inflow points the pressure and velocity were specified and the characteristic value of the incoming characteristic was used to calculate the density. The energy equation is used to calculate the energy. (Even though characteristic boundary conditions were used for the colliding shock problem, this fourth-order smoothing was not able to control Gibbs oscillations emanating from the subsonic inflow boundary. A second-order scheme was required in the neighborhood of that boundary to keep those oscillations under control. Without it the computed solution rapidly diverged from the analytic solution at the boundary.)

The initial conditions are shown in Figures 9 through 12. Results for the first case are shown in Figures 13 through 24 . The analytic solution is shown for comparison by the solid lines. For this case the shock waves intersect at $t \approx .057$. These conditions have been chosen so that, after the intersection, the shock on the left is propagating to the left with

respect to ground-fixed coordinates in case 1 and to the right in case 2. The arrows which appear in all post-intersection figures are used only to indicate the direction of propagation of each shock with respect to a ground fixed frame of reference and bear no relation to other shock characteristics. As previously mentioned the two post-intersection shock waves travel in opposite directions for this case.

The solution at post collision times is plotted in Figures 17 through 24, corresponding to the 2000th, 4000th and 6000th iterations respectively. The solid lines represent the analytic solution. Agreement in the position of the discontinuities between the analytic and computed solutions is very good. At the 2000th iteration the agreement with the flow variables in the region between the two shock waves is only fair since only five points lie in this zone at this time. However, as the number of iterations increase and this zone becomes larger (i.e. more points lie within it), the agreement becomes very good. By the 4000th iteration, the computed values of flow variables exactly match the analytic values.

The difference in resolution of the two shock waves is due to two factors. The first is that the artificial viscosity constant cannot be tailored to both shocks, which are of different strengths. The value used herein was selected to provide maximum resolution of the stronger shock while producing minimum rounding of the weaker shock. As can be seen in the figures there is some minor rounding of the weaker shock wave. The second and more significant reason is that the physical space point resolution is not constant. It is greatest at $x = \pm 1$ and least at $x = 0.0$. The weaker shock in this case always lies in the neighborhood of $x = 0.0$, the minimum point resolution zone. This is why the computed shock front of the weaker shock is not as steep as for the stronger shock wave.

The pseudospectral resolution characteristics of the contact discontinuity are not as good as those of the shock waves. Part of this is due to the above mentioned unequal point spacing. However, most is due to the nature of the solution scheme together with the significant difference in the physical nature of the two types of discontinuities. Shock waves yield discontinuous values of all flow variables across their front while contact

surface discontinuities yield jumps in density and energy alone.

Results for the second case are shown in Figures 25 through 40 . There are several important differences between this case and the first. The initial shock strengths are such that, after intersection, both shock waves move to the right with respect to ground fixed coordinates. Further, the difference in post intersection shock strengths is greater in this case. Perhaps the major difference, however, is in the initial positions of the shocks. In the first case both were far away from the computational boundaries. In this case it was decided to purposely place one shock much closer to a boundary to see what, if any, effect this would have on the properties of the solution. The left hand shock was placed only twenty points from the computational boundary. No adverse results were observed.

As in the first case, the comparison with the analytic solution is very good. All shocks are resolved as sharp discontinuities and at the correct position. The contact surface resolution was as before not as good, being spread over four to five collocation points, though centered about the analytic location.

V. CONCLUSIONS

The central conclusion is that the pseudospectral solution technique together with a fourth-order artificial viscosity smoothing scheme works just as well for cases where multiple discontinuities are present as it does when only a single discontinuity is present. The resolution of contact surface discontinuities is not as good as that for shock discontinuities, the former being spread over four to five grid or collocation points as compared to two to three grid points (one to two grid intervals for the latter).

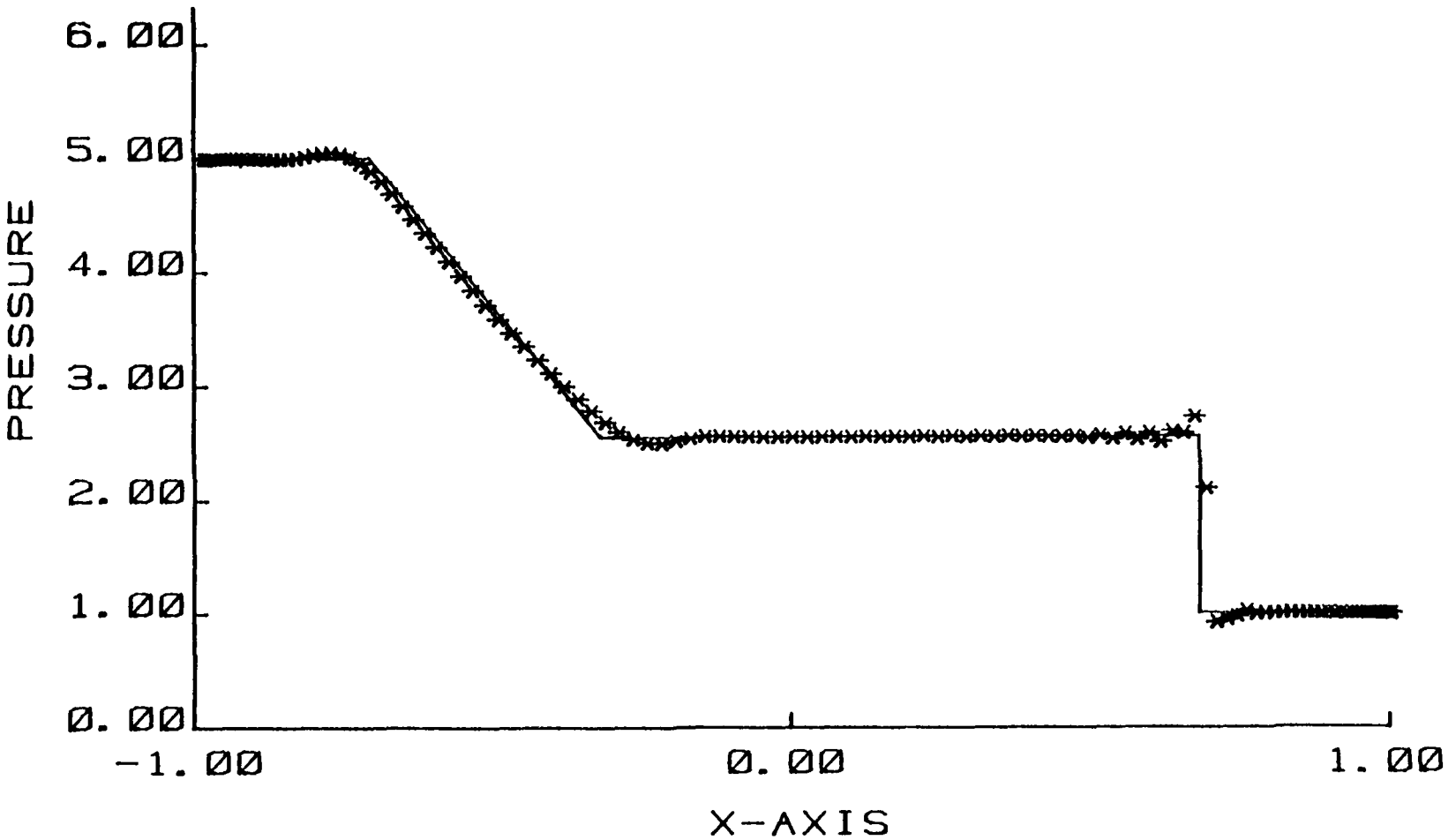

Figure 1 Bursting Diaphragm Flow Pressure Field, Case 1.

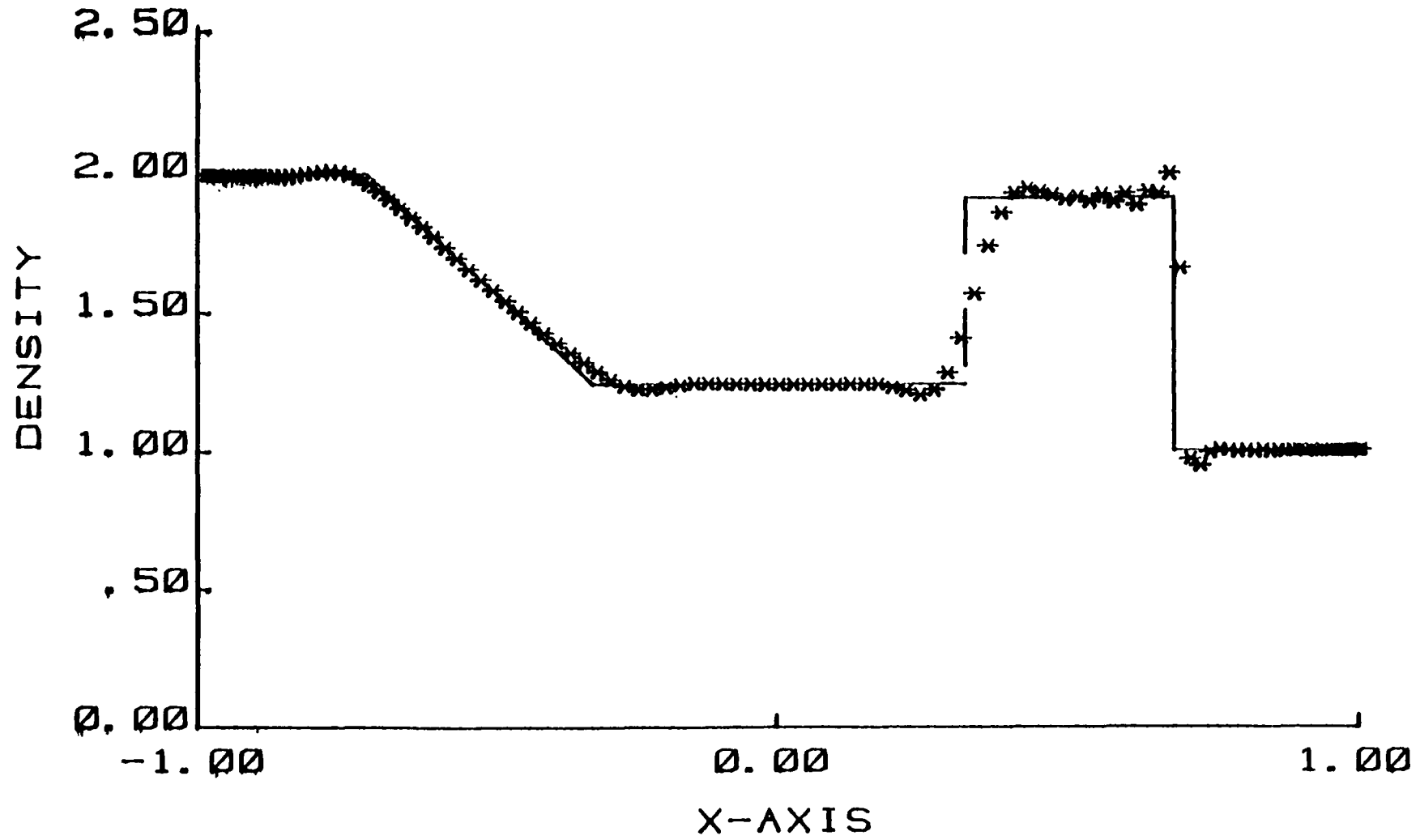

Figure 2 Bursting Diaphragm Flow Density Field, Case 1.

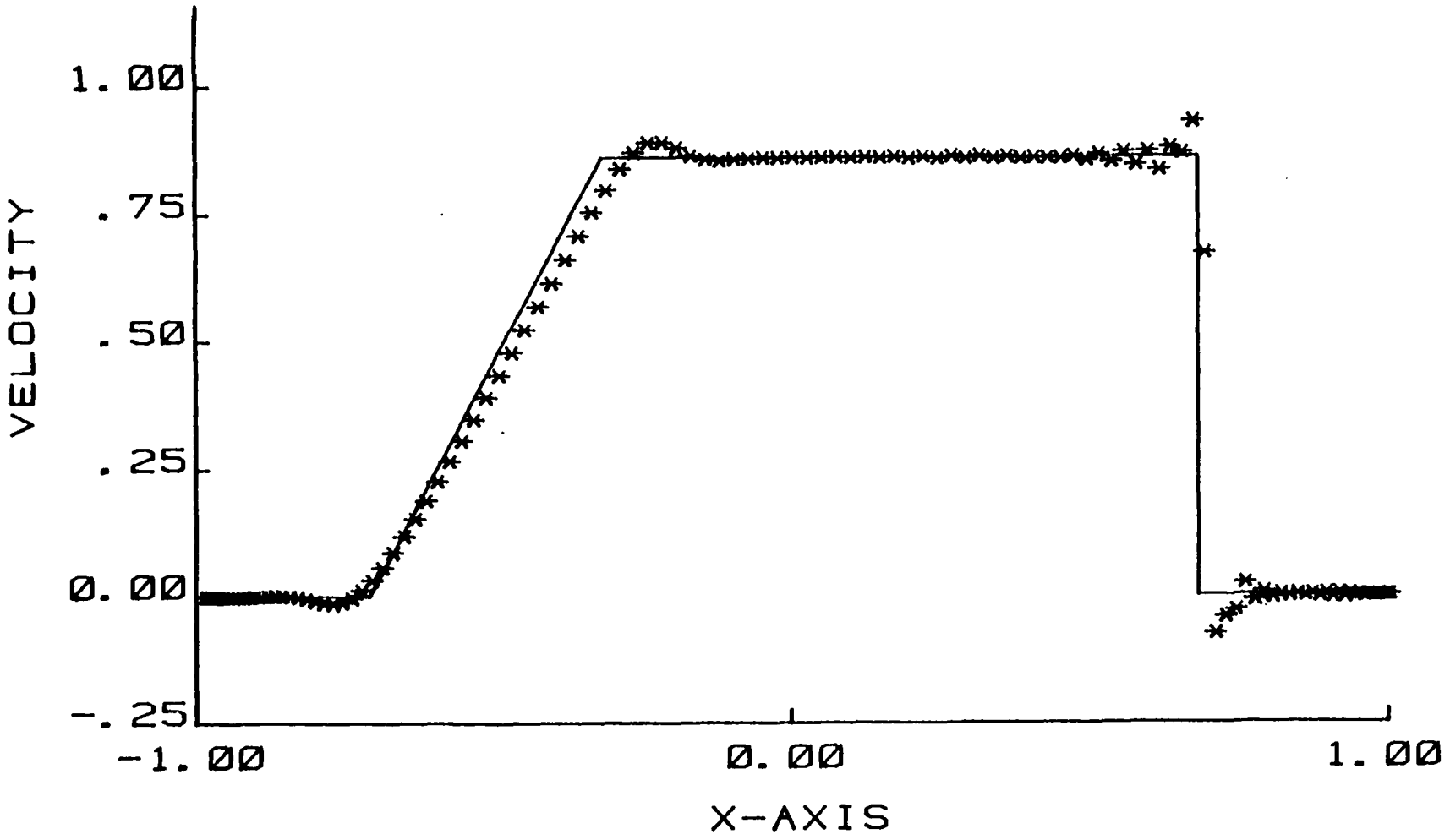

Figure 3 Bursting Diaphragm Flow Velocity Field, Case 1.

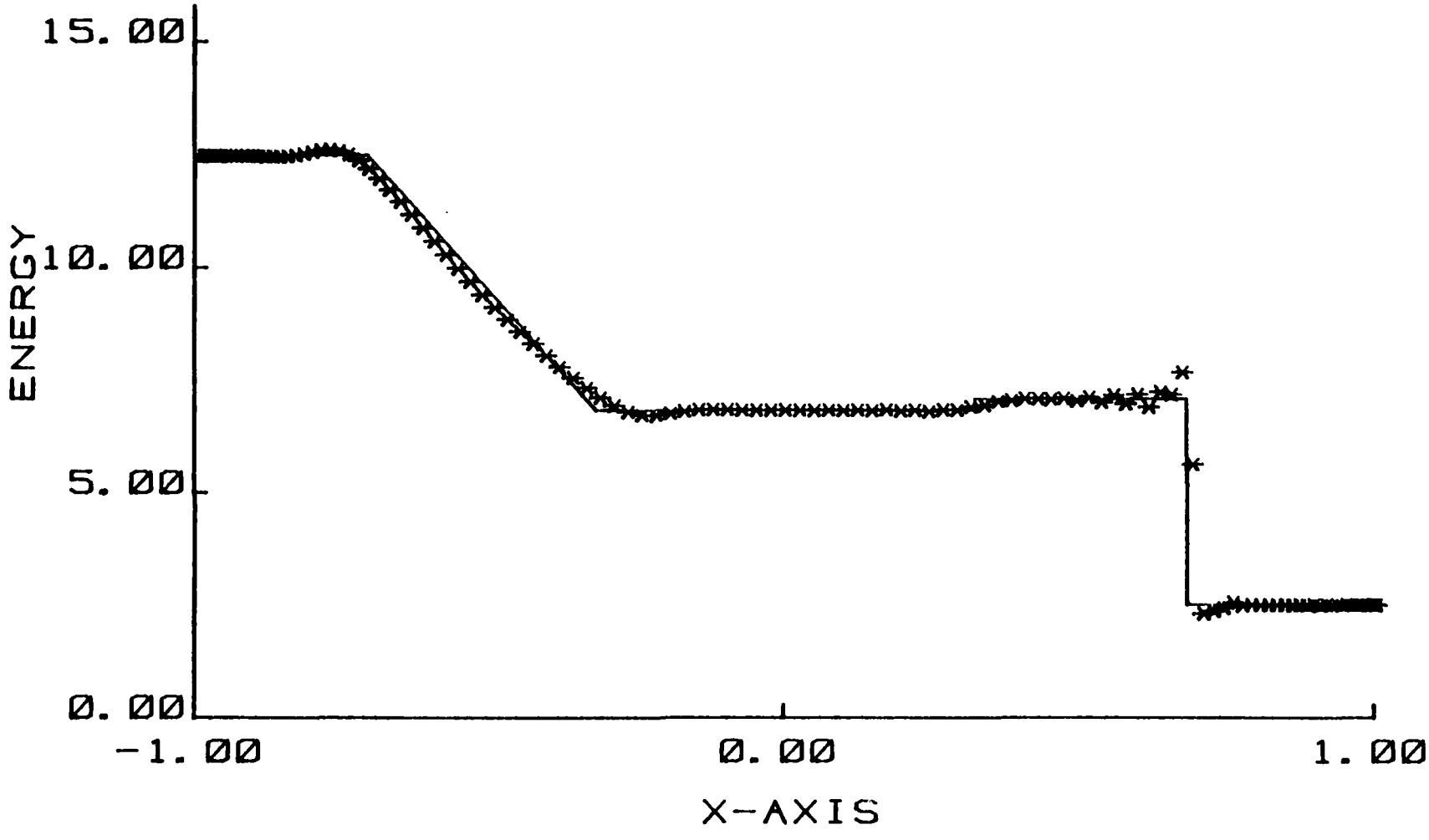

Figure 4 Bursting Diaphragm Flow Energy Field, Case 1.

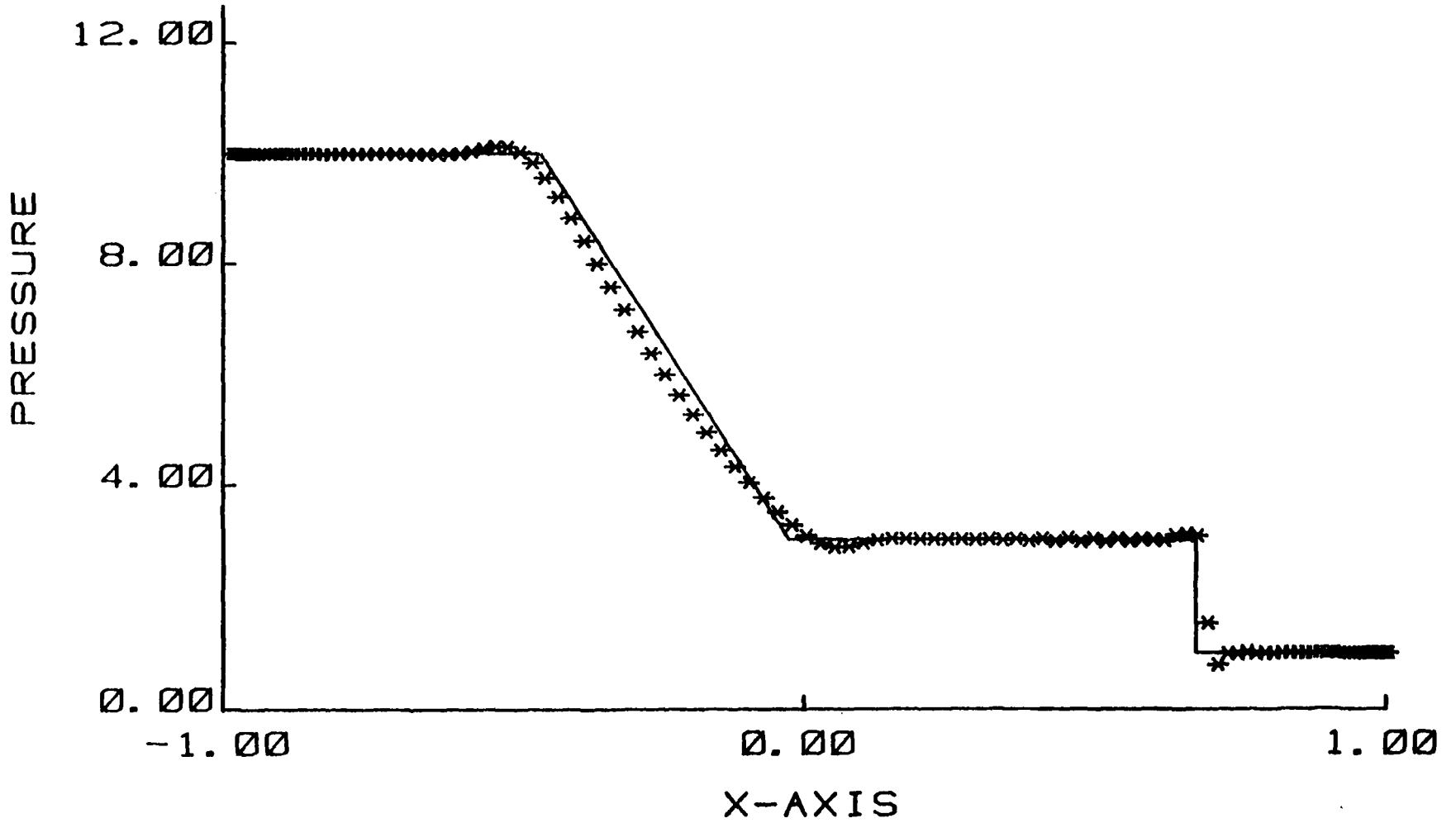

Figure 5 Bursting Diaphragm Flow Pressure Field, Case 2.

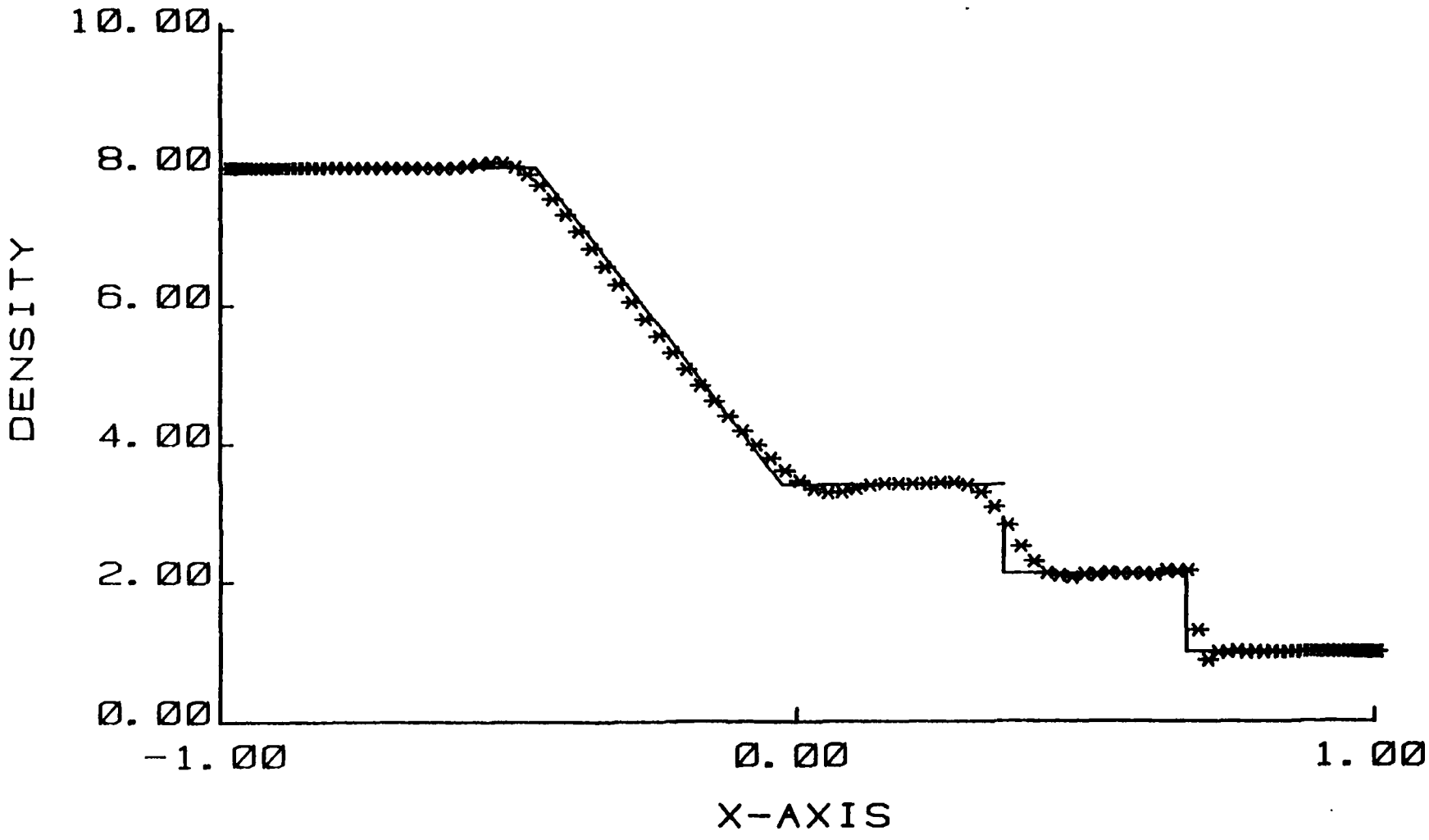

Figure 6 Bursting Diaphragm Flow Density Field, Case 2.

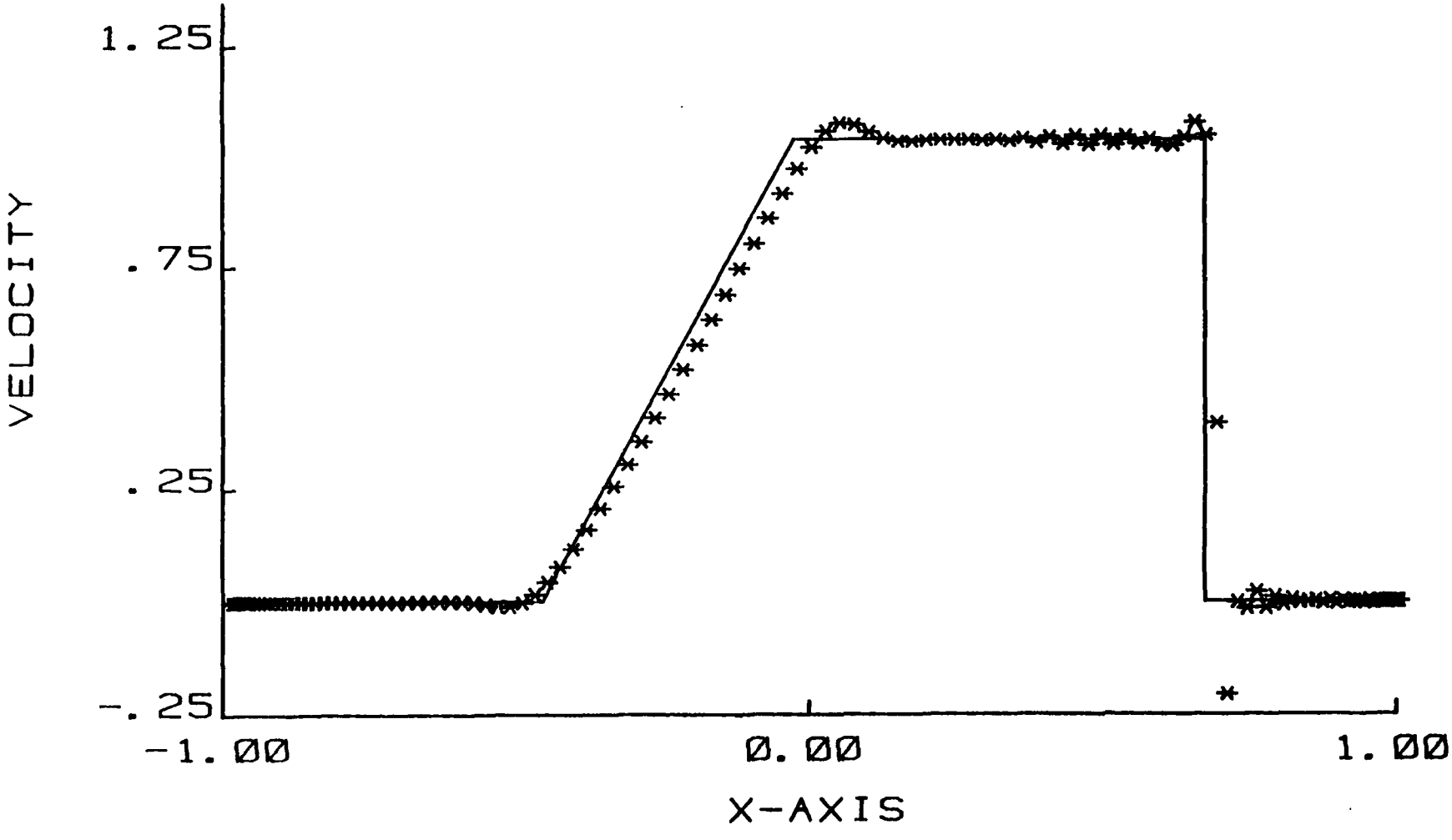

Figure 7 Bursting Diaphragm Flow Velocity Field, Case 2.

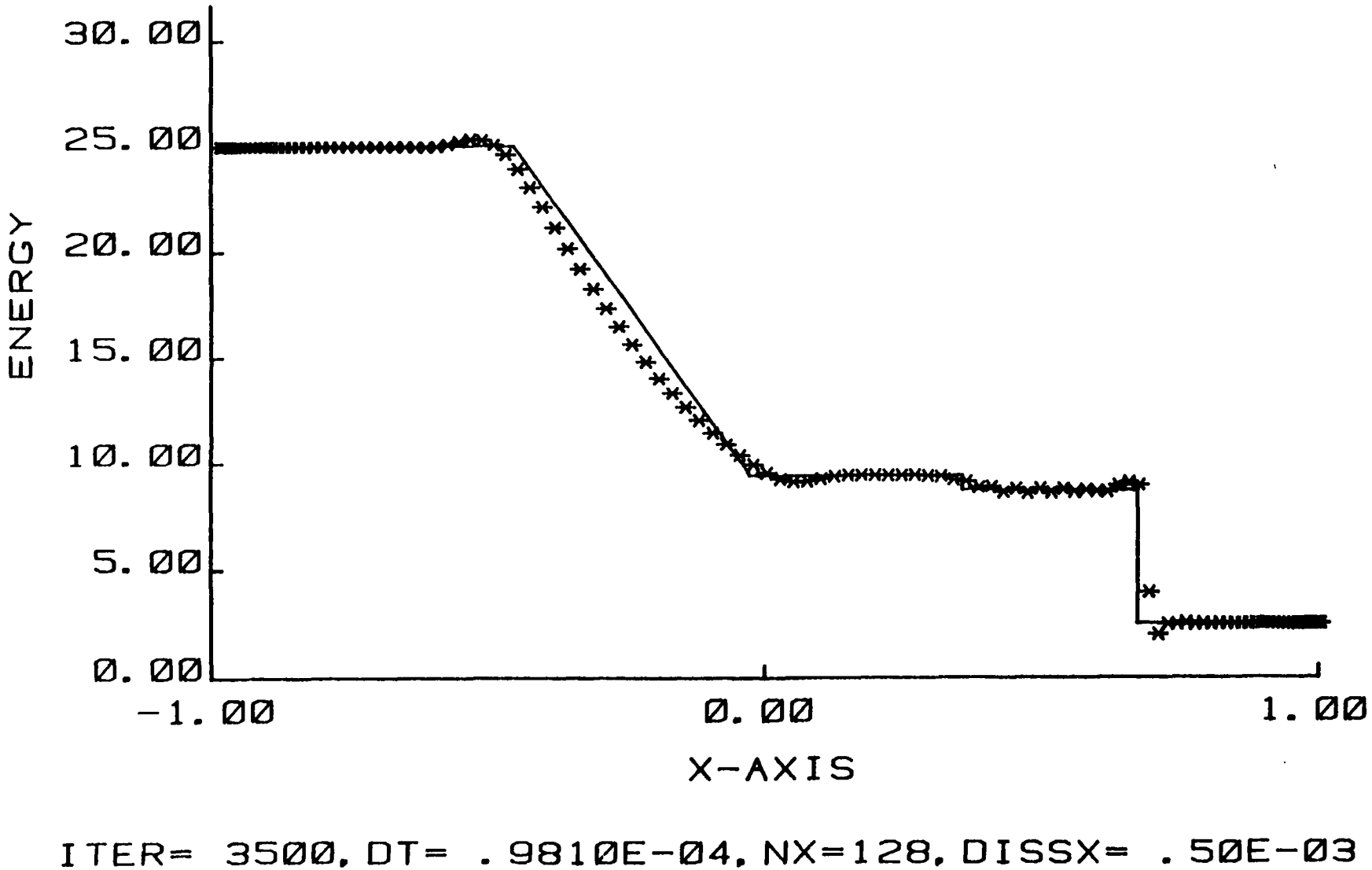

Figure 8 Bursting Diaphragm Flow Energy Field, Case 2.

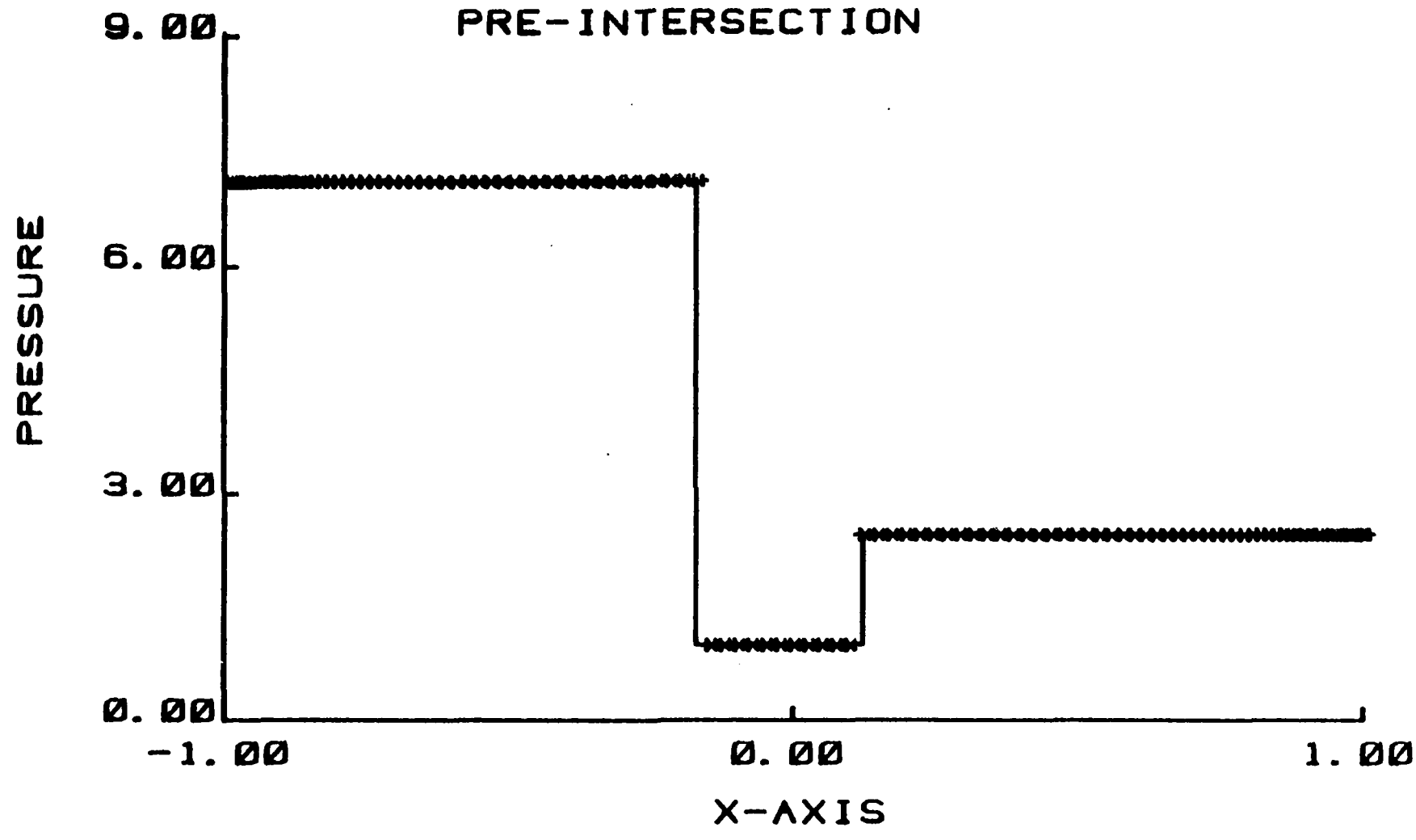

Figure 9 Colliding Shock Waves, Initial Pressure Field, Case 1.

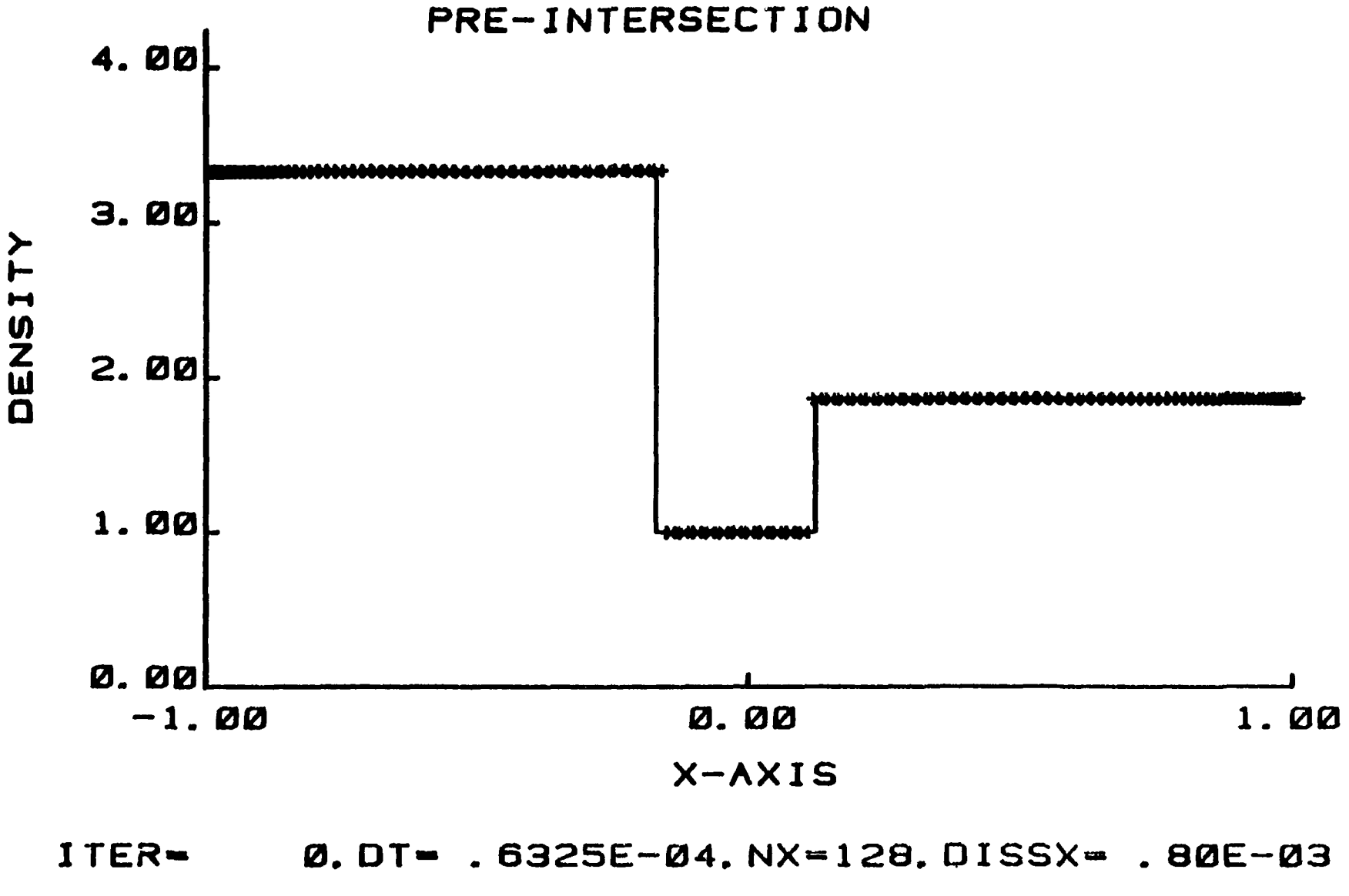

Figure 10 Colliding Shock Waves, Initial Density Field, Case 1.

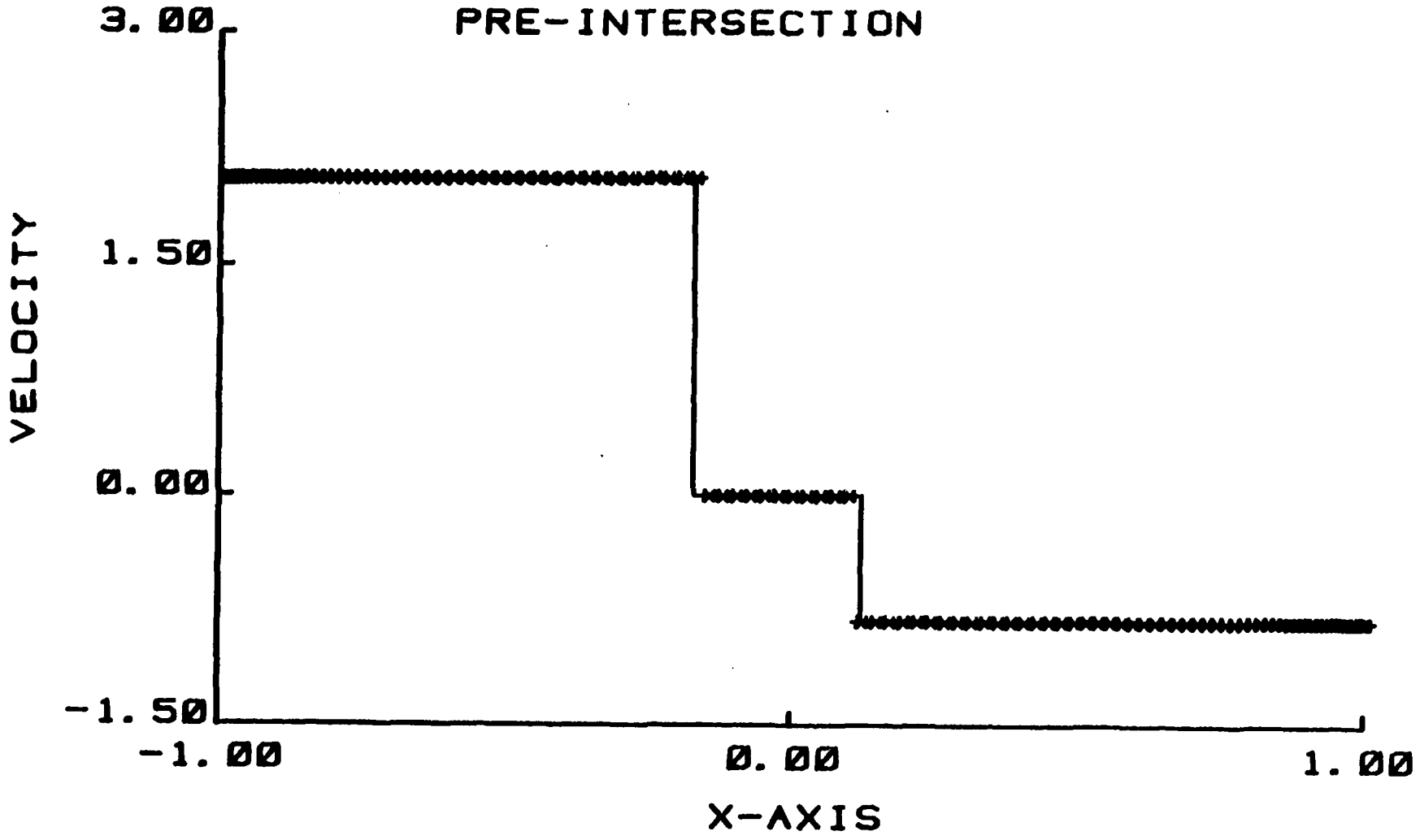

Figure 11 Colliding Shock Waves, Initial Velocity Field, Case 1.

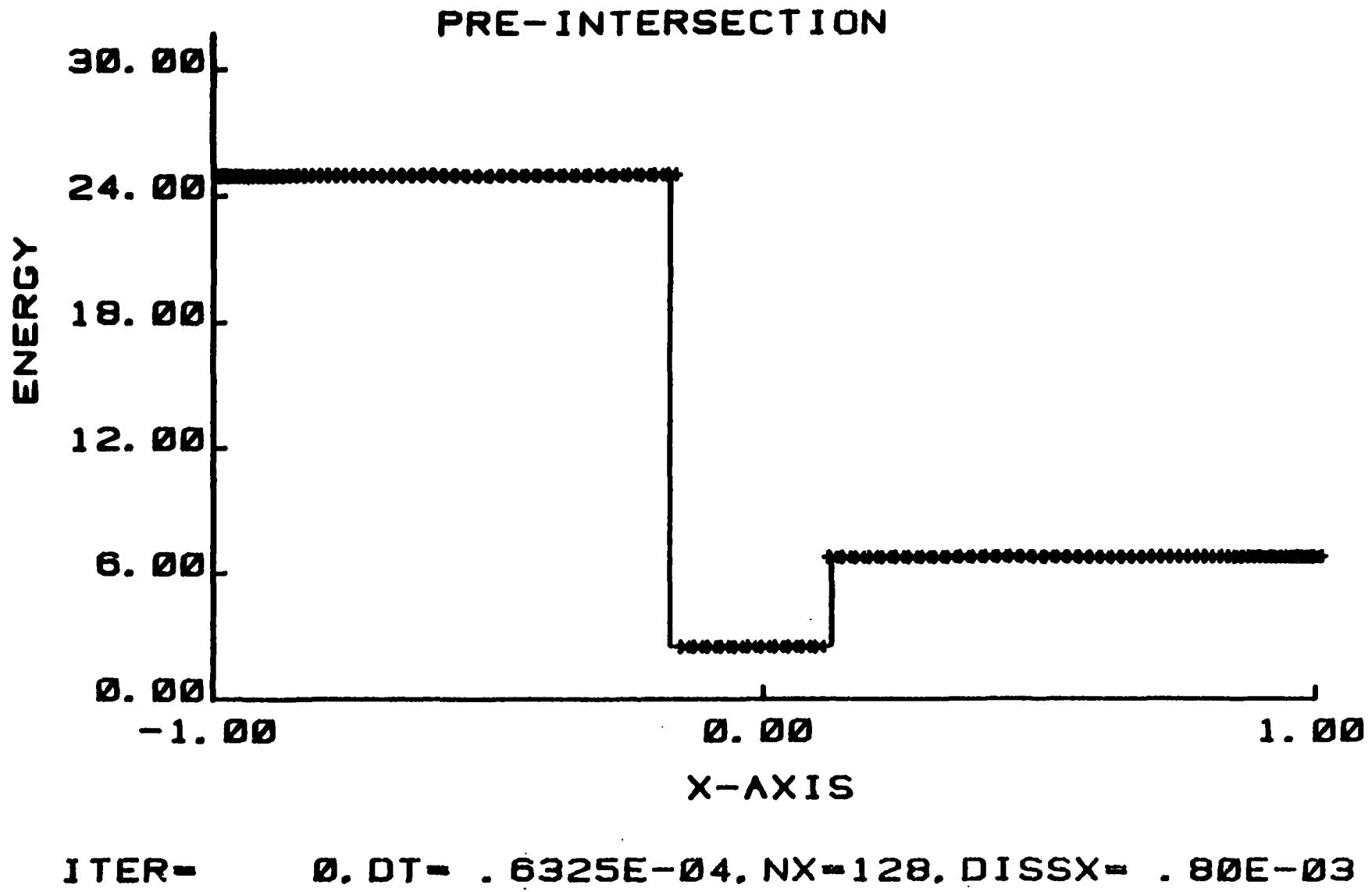

Figure 12 Colliding Shock Waves, Initial Energy Field, Case 1.

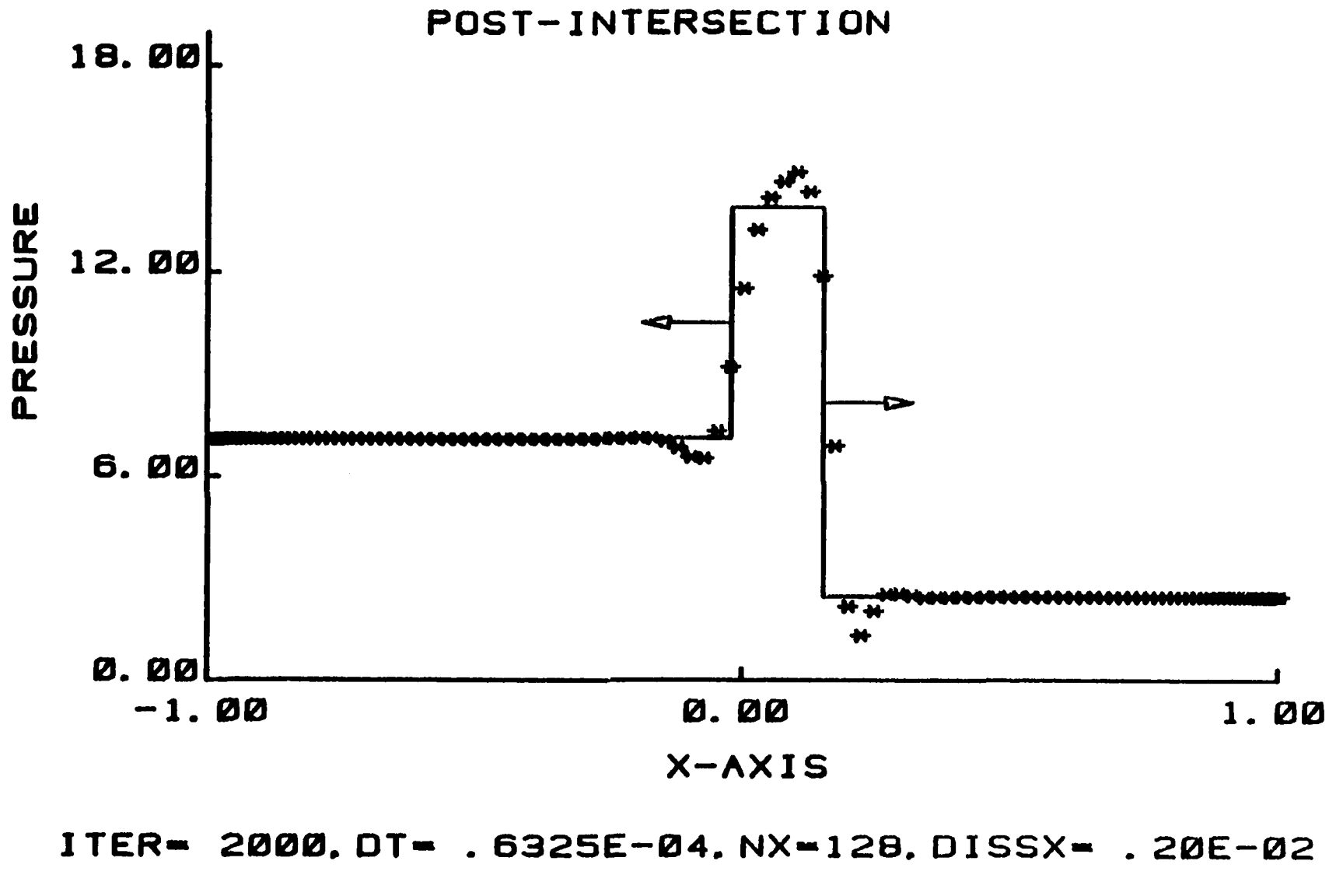

Figure 13 Colliding Shock Waves, Post-Collision Pressure Field, Case 1.

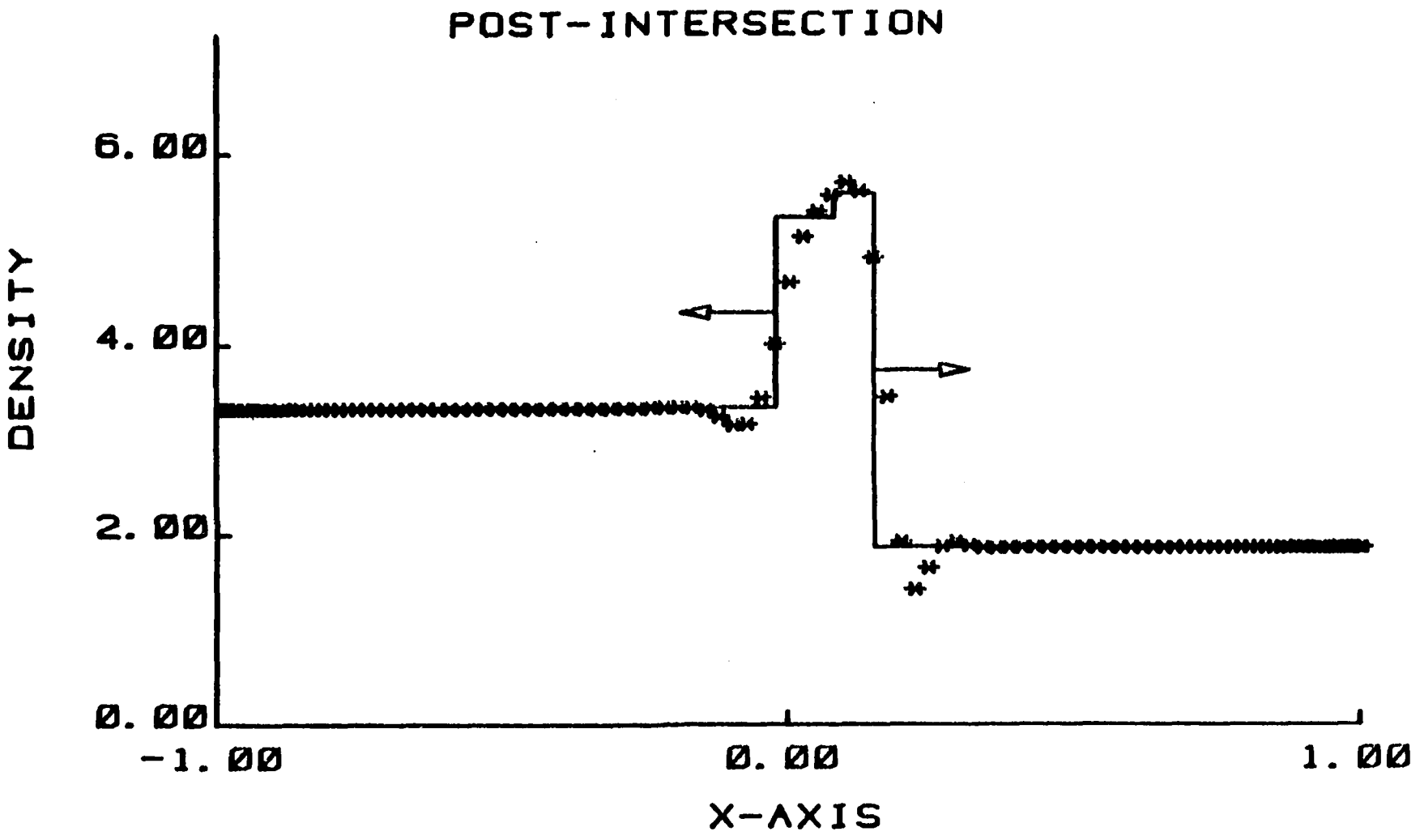

Figure 14 Colliding Shock Waves, Post-Collision Density Field, Case 1.

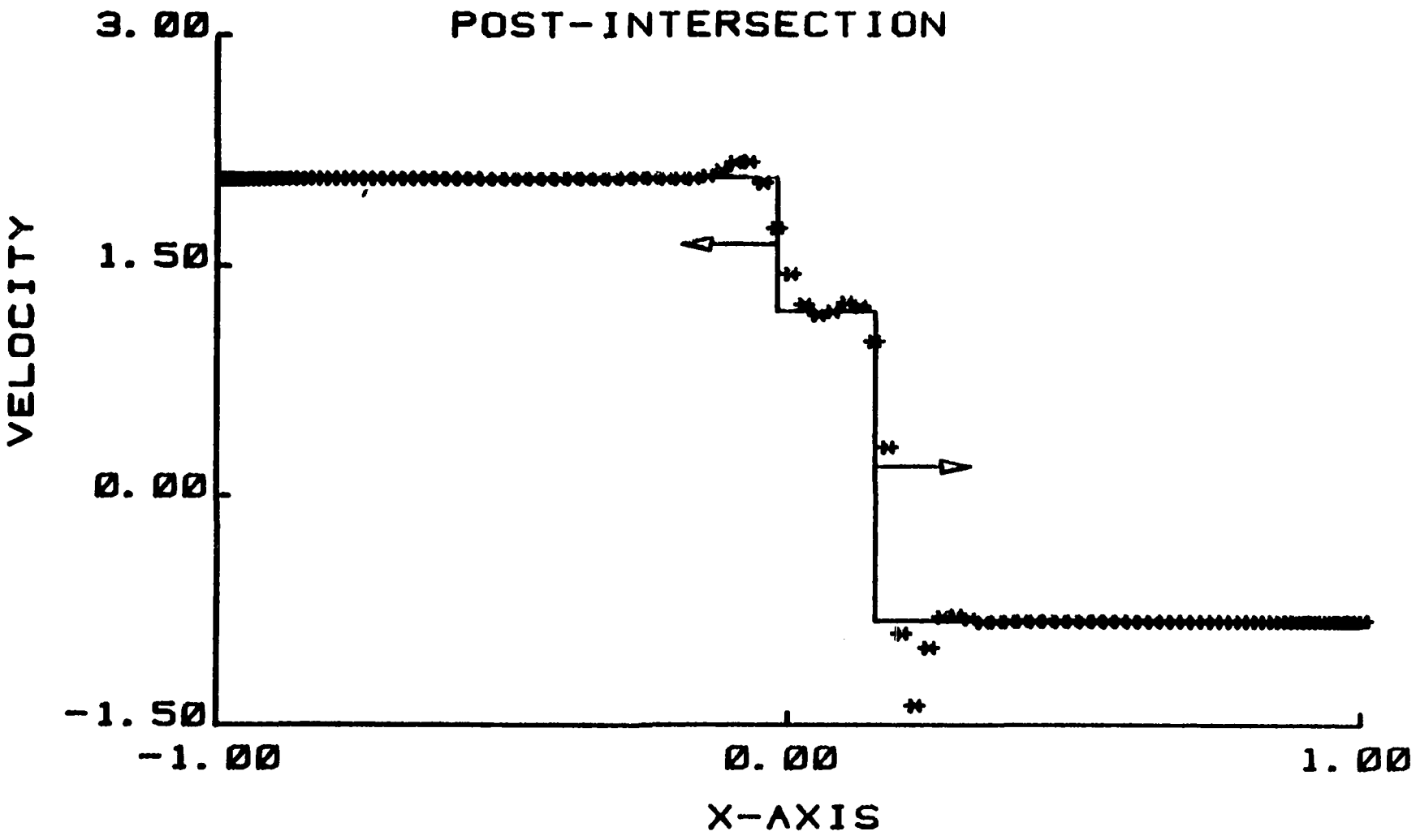

Figure 15 Colliding Shock Waves, Post-Collision Velocity Field, Case 1.

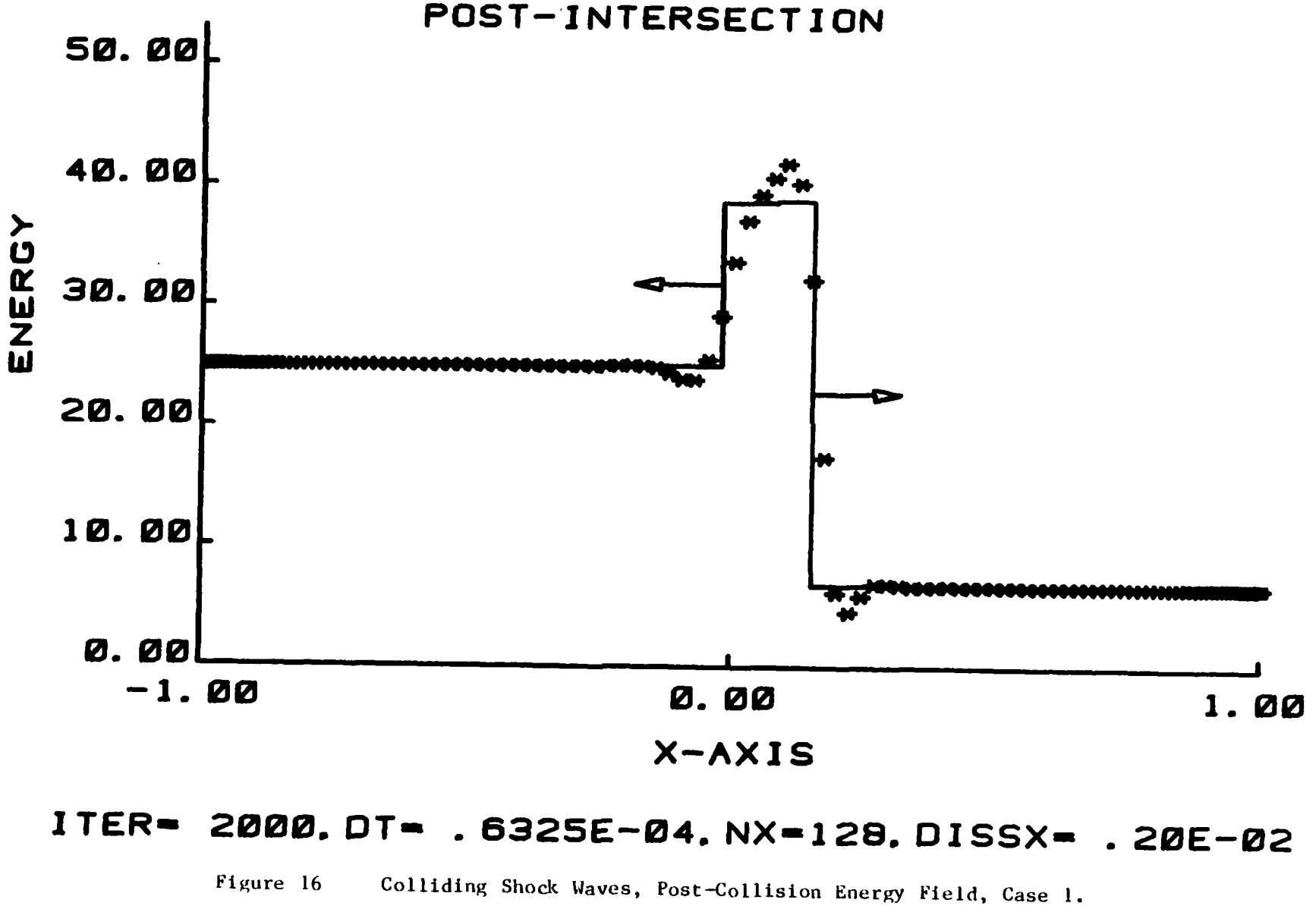

Figure 16 Colliding Shock Waves, Post-Collision Energy Field, Case 1.

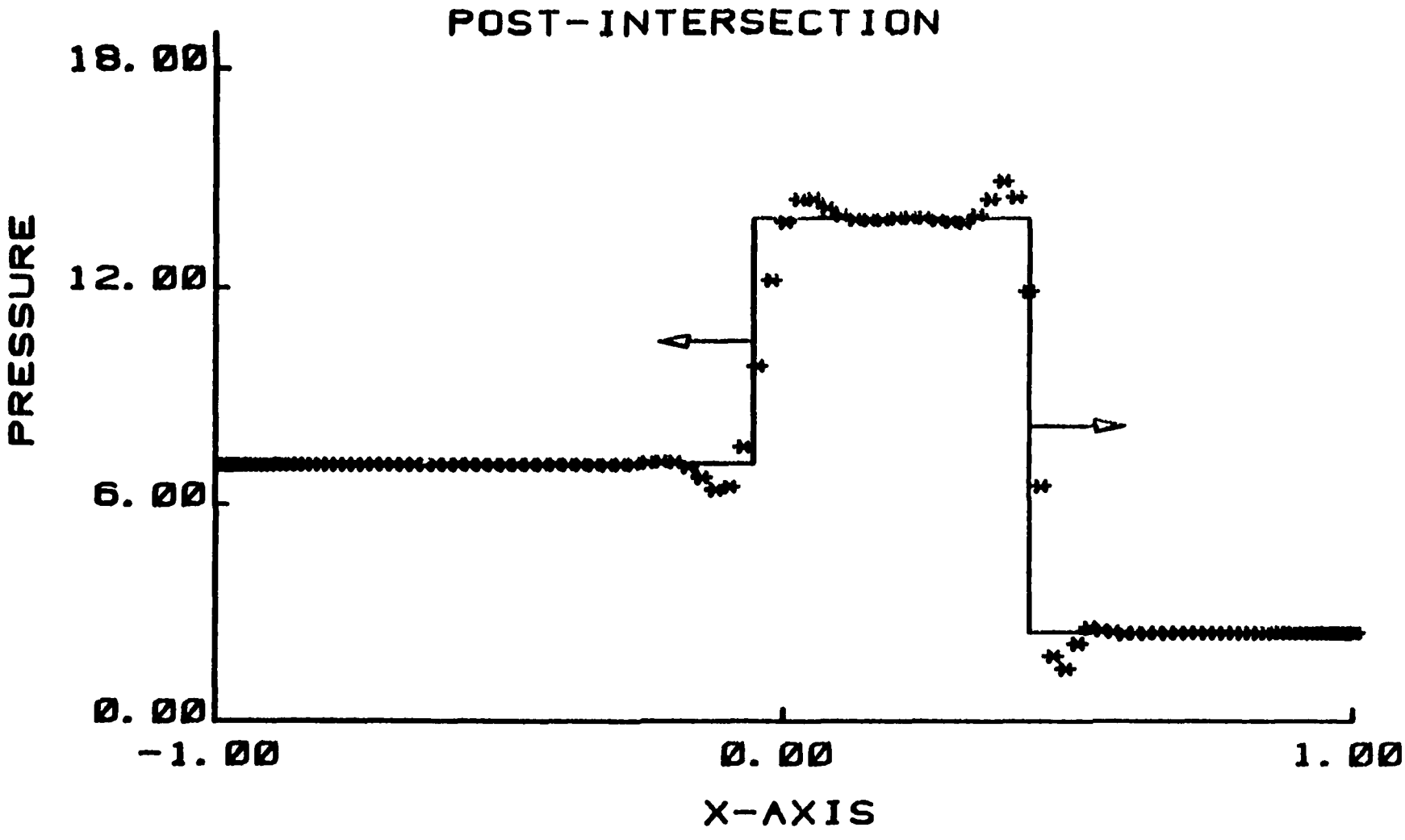

Figure 17 Colliding Shock Waves, Post-Collision Pressure Field, Case 1.

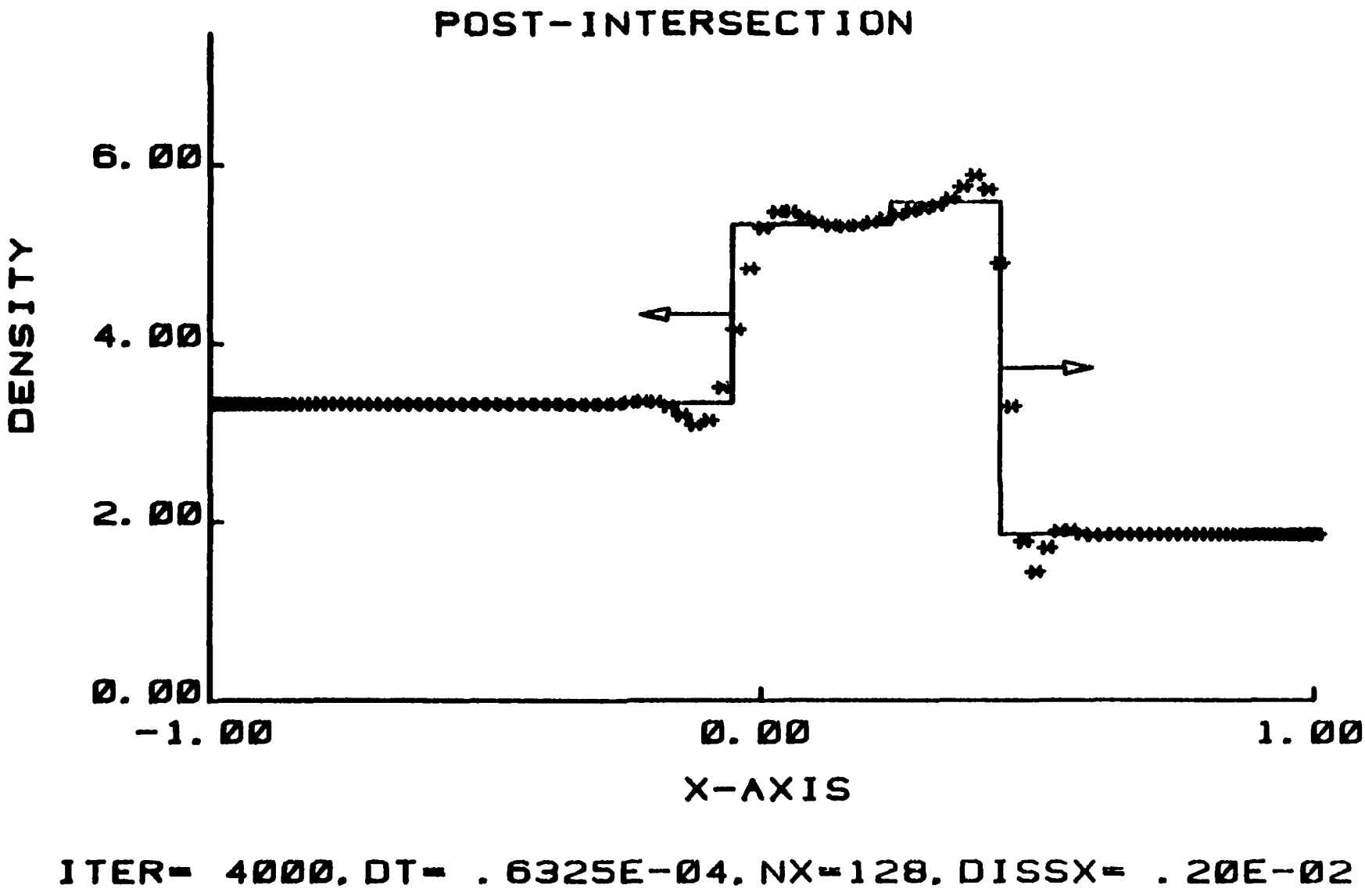

Figure 18 Colliding Shock Waves, Post-Collision Density Field, Case 1.

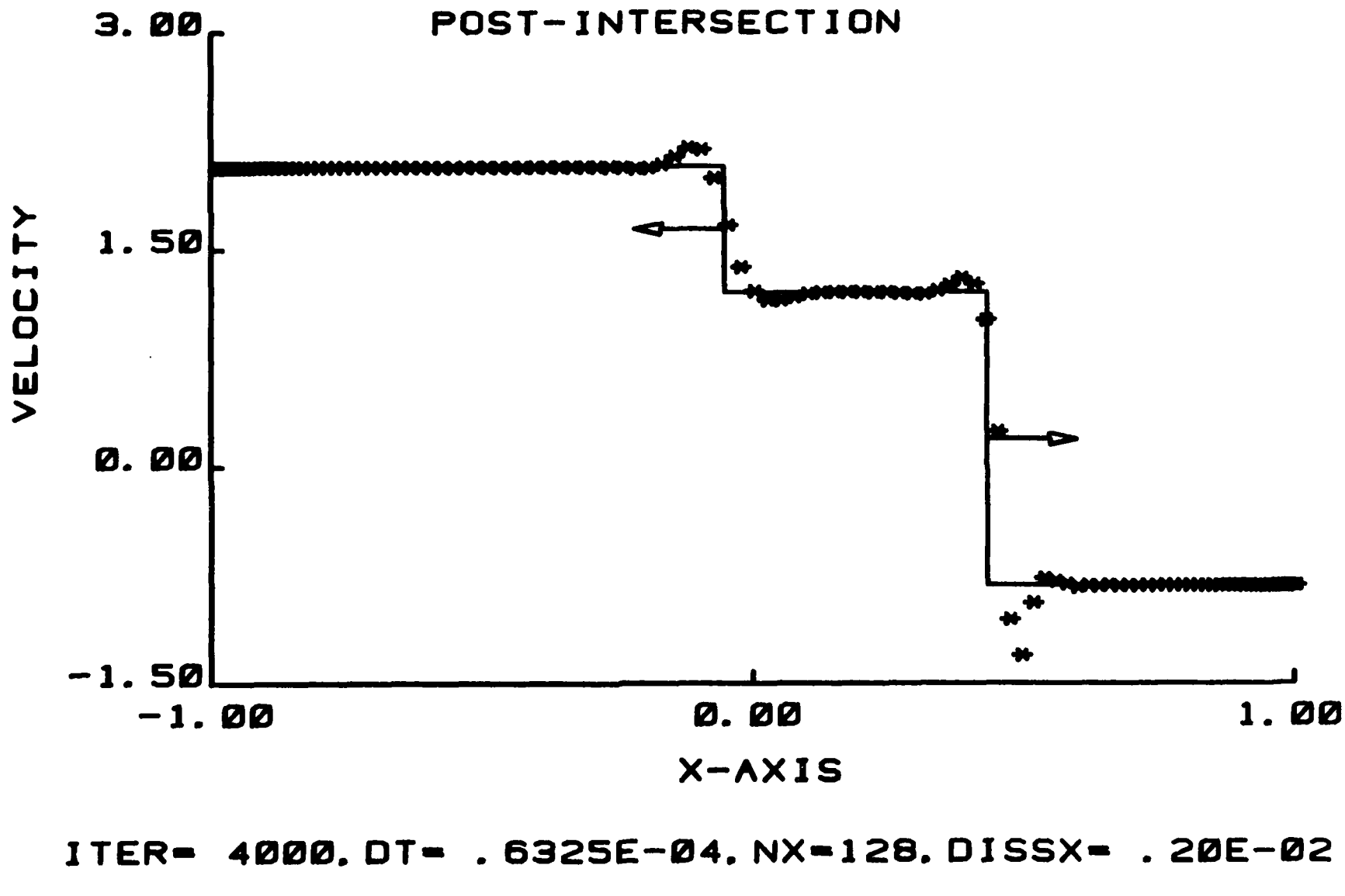

Figure 19 Colliding Shock Waves, Post-Collision Velocity Field, Case 1.

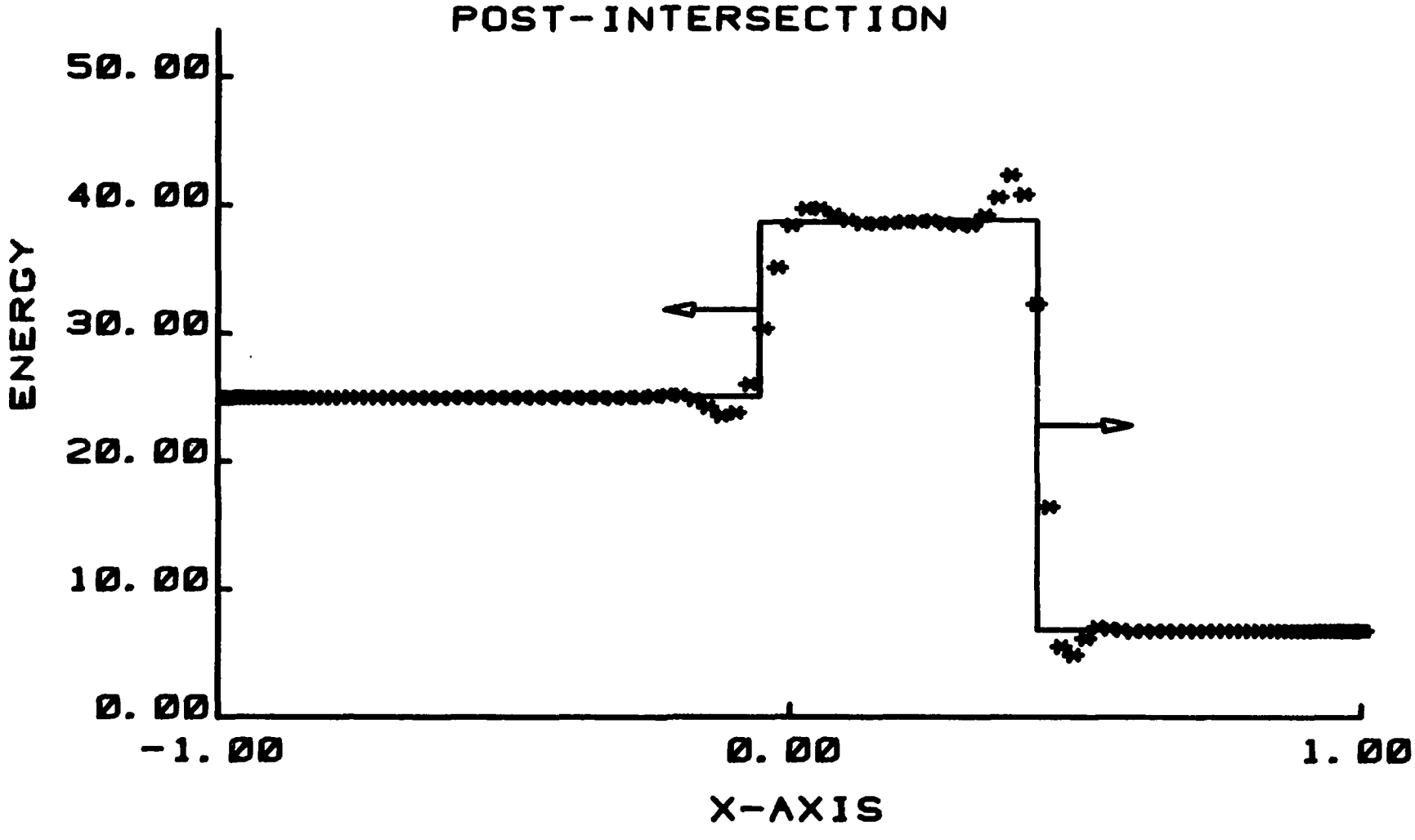

Figure 20 Colliding Shock Waves, Post-Collision Energy Field, Case 1.

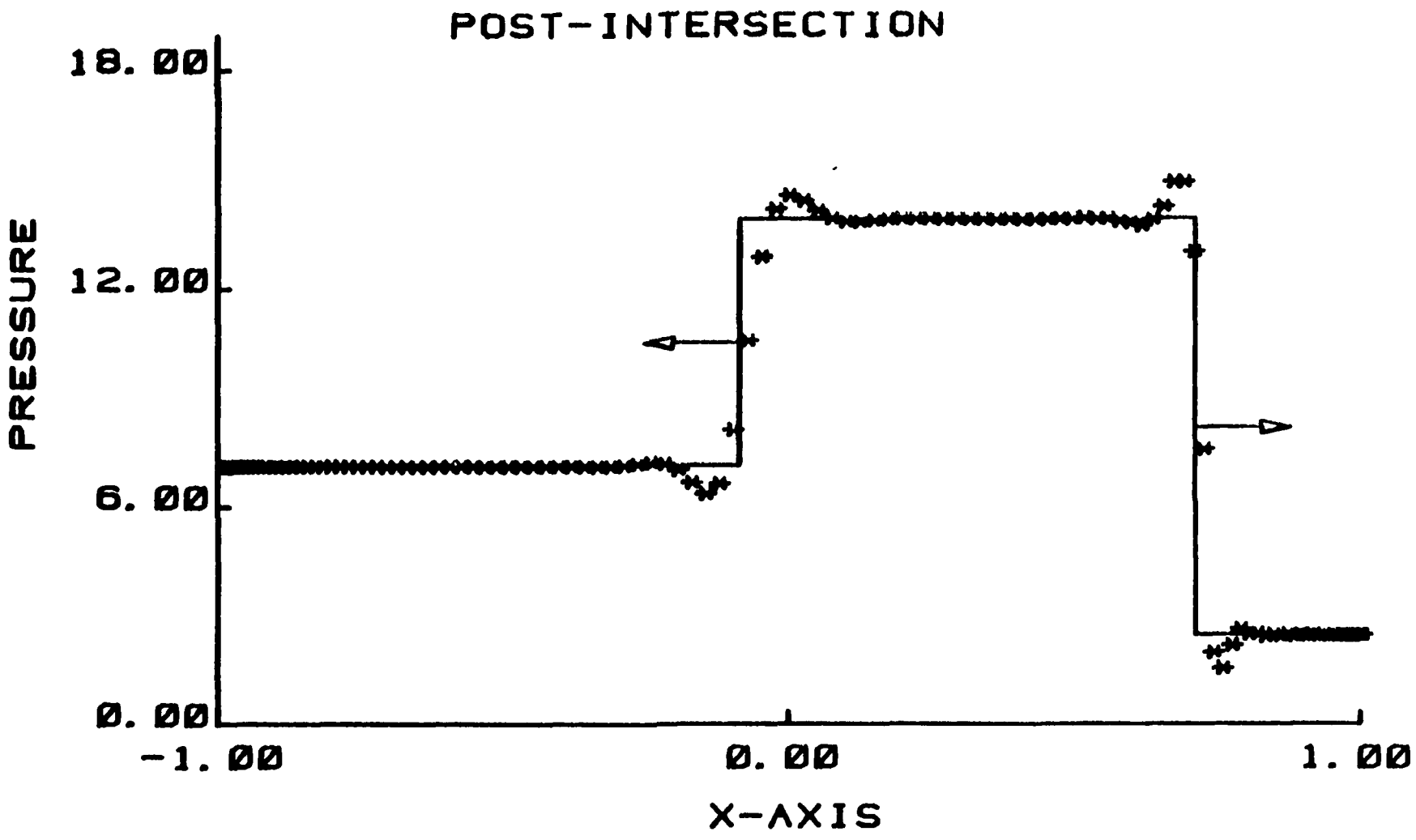

Figure 21 Colliding Shock Waves, Post-Collision Pressure Field, Case 1.

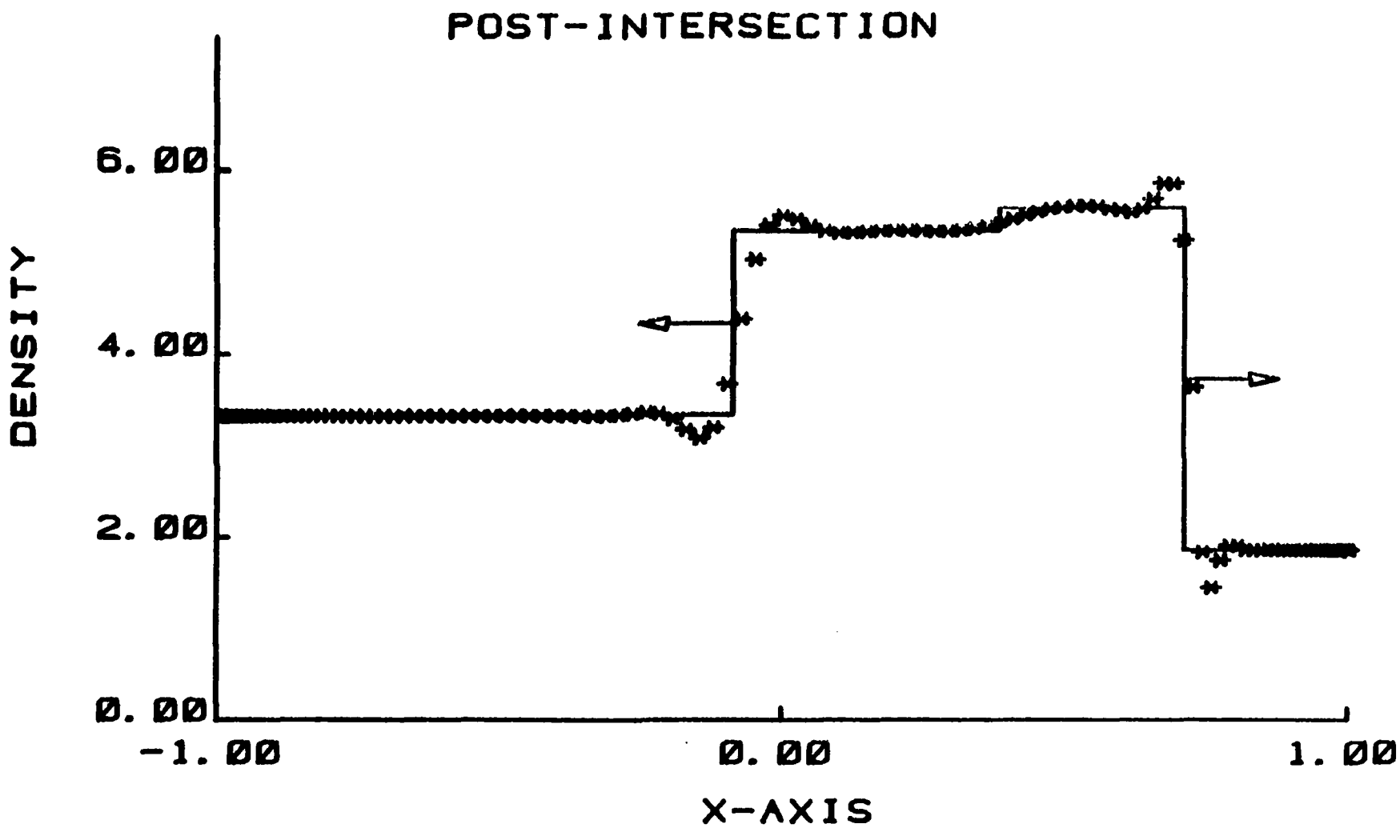

Figure 22 Colliding Shock Waves, Post-Collision Density Field, Case 1.

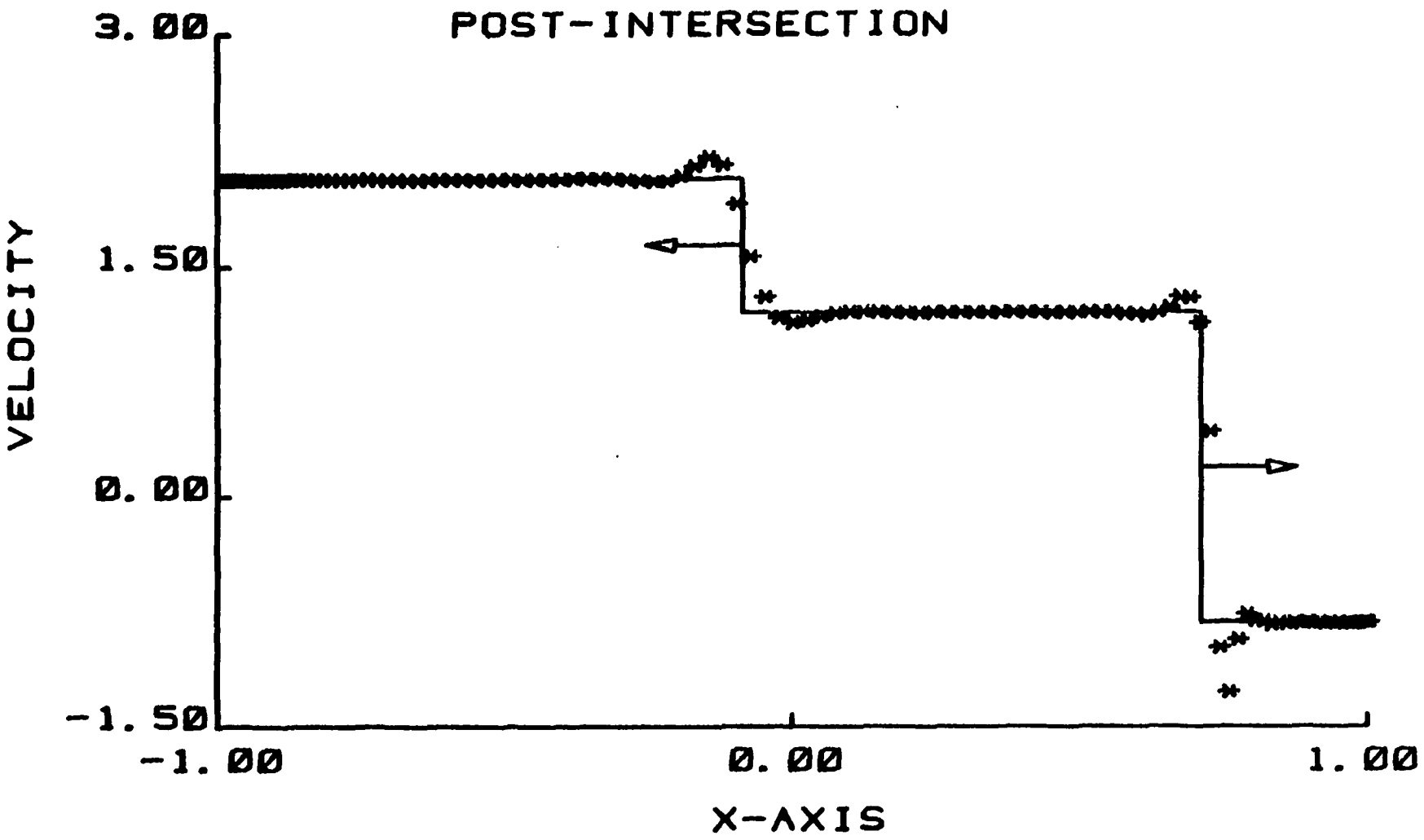

Figure 23 Colliding Shock Waves, Post-Collision Velocity Field, Case 1.

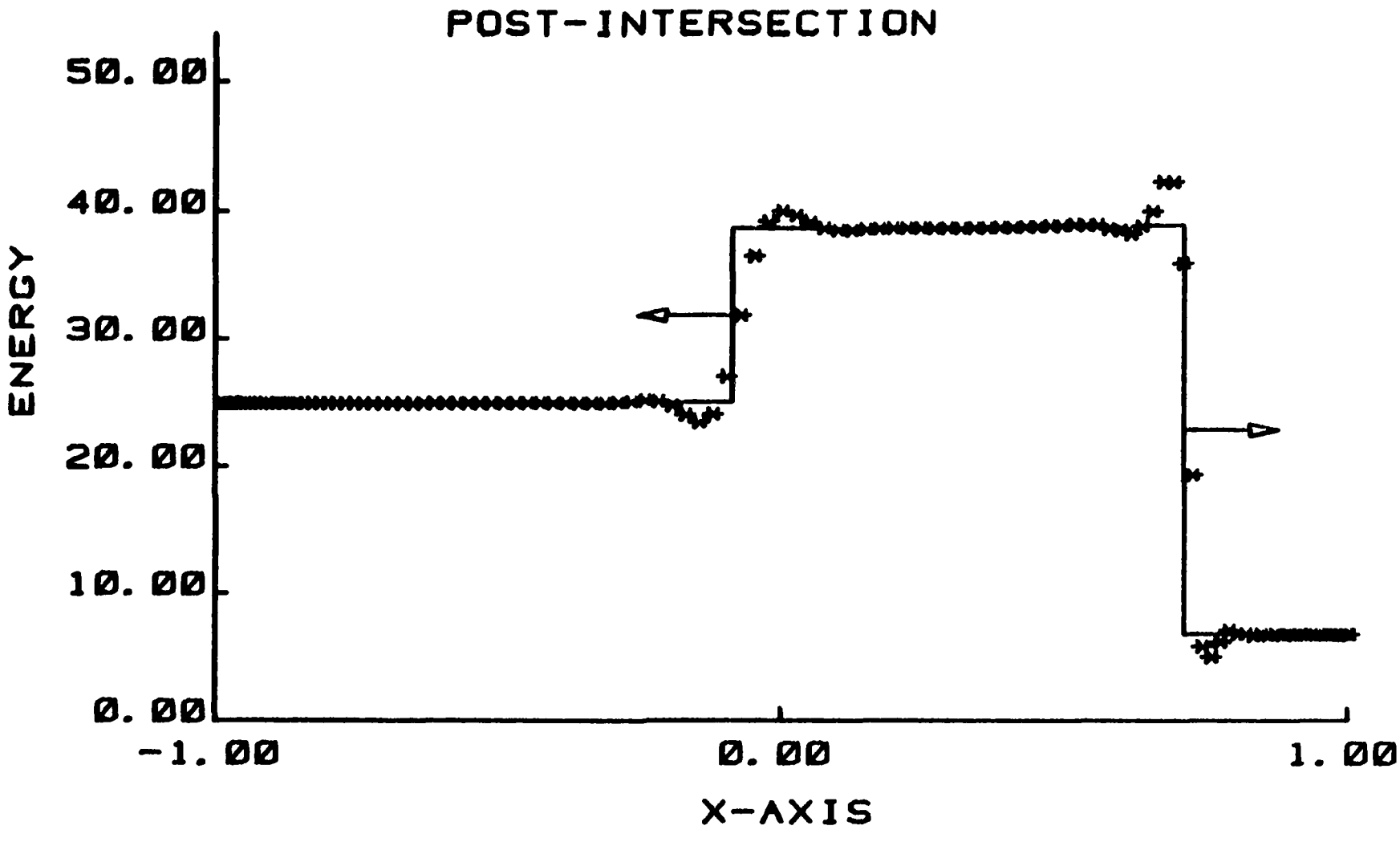

Figure 24 Colliding Shock Waves, Post-Collision Energy Field, Case 1.

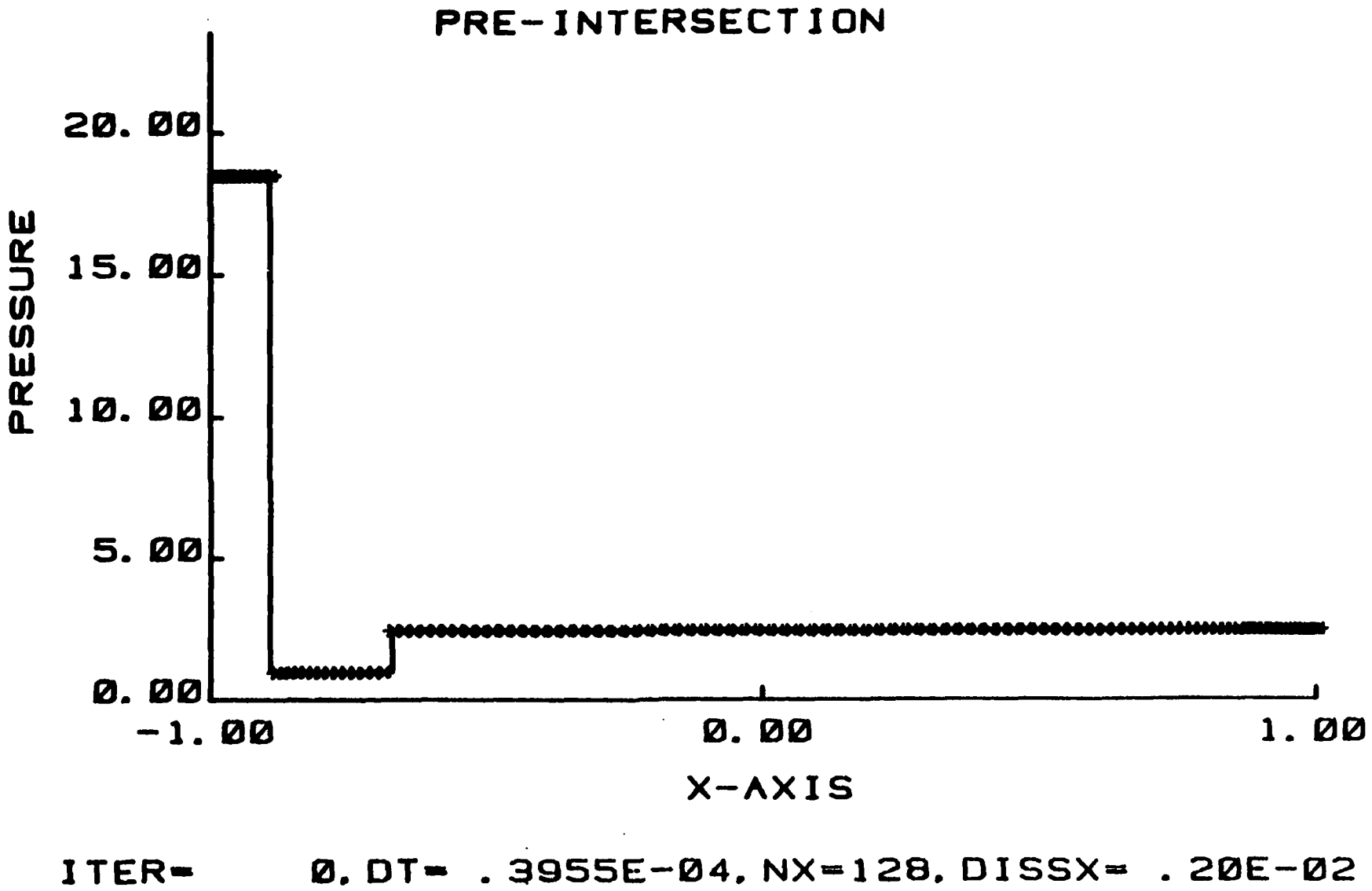

Figure 25 Colliding Shock Waves; Initial Pressure Field, Case 2.

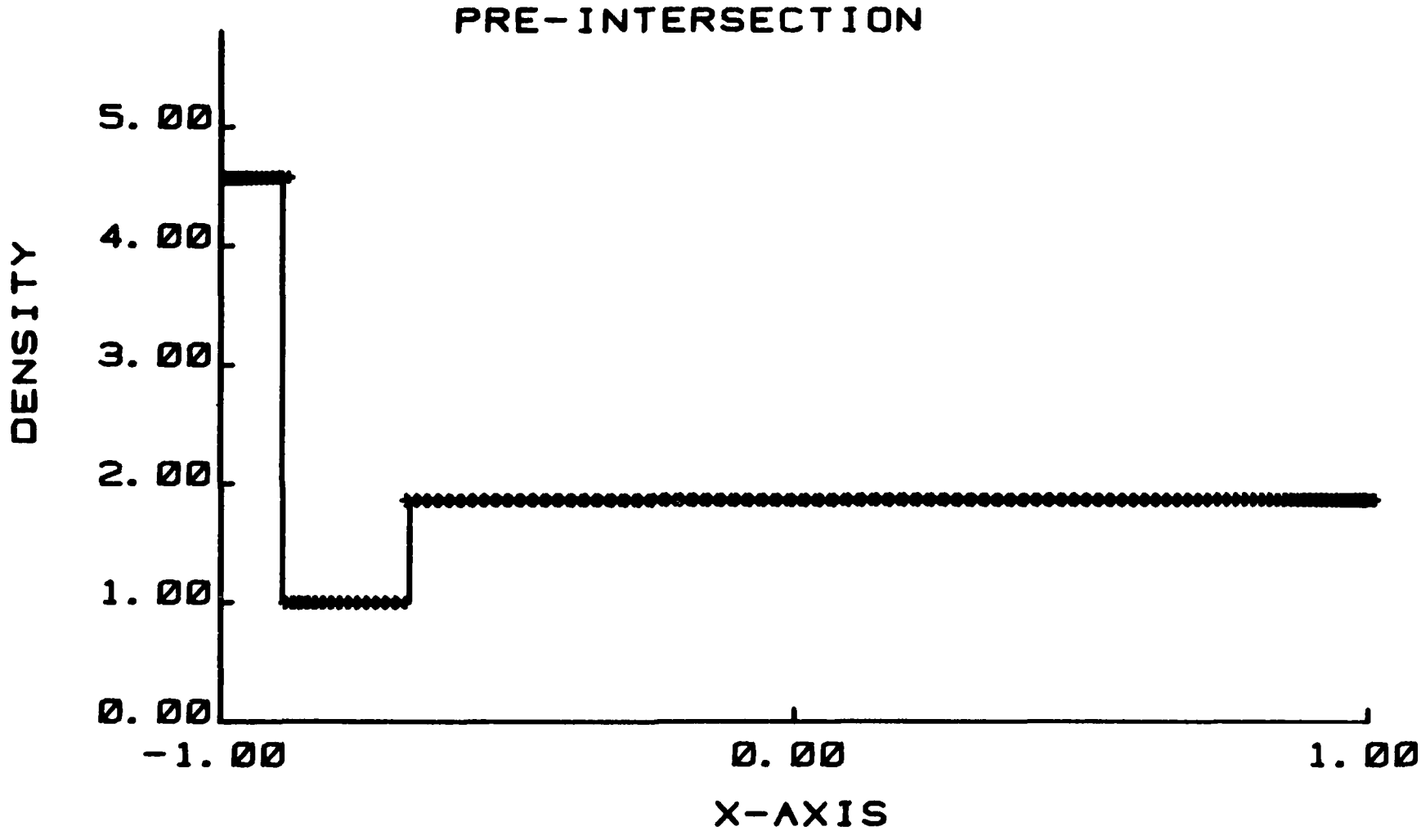

Figure 26 Colliding Shock Waves; Initial Density Field, Case 2.

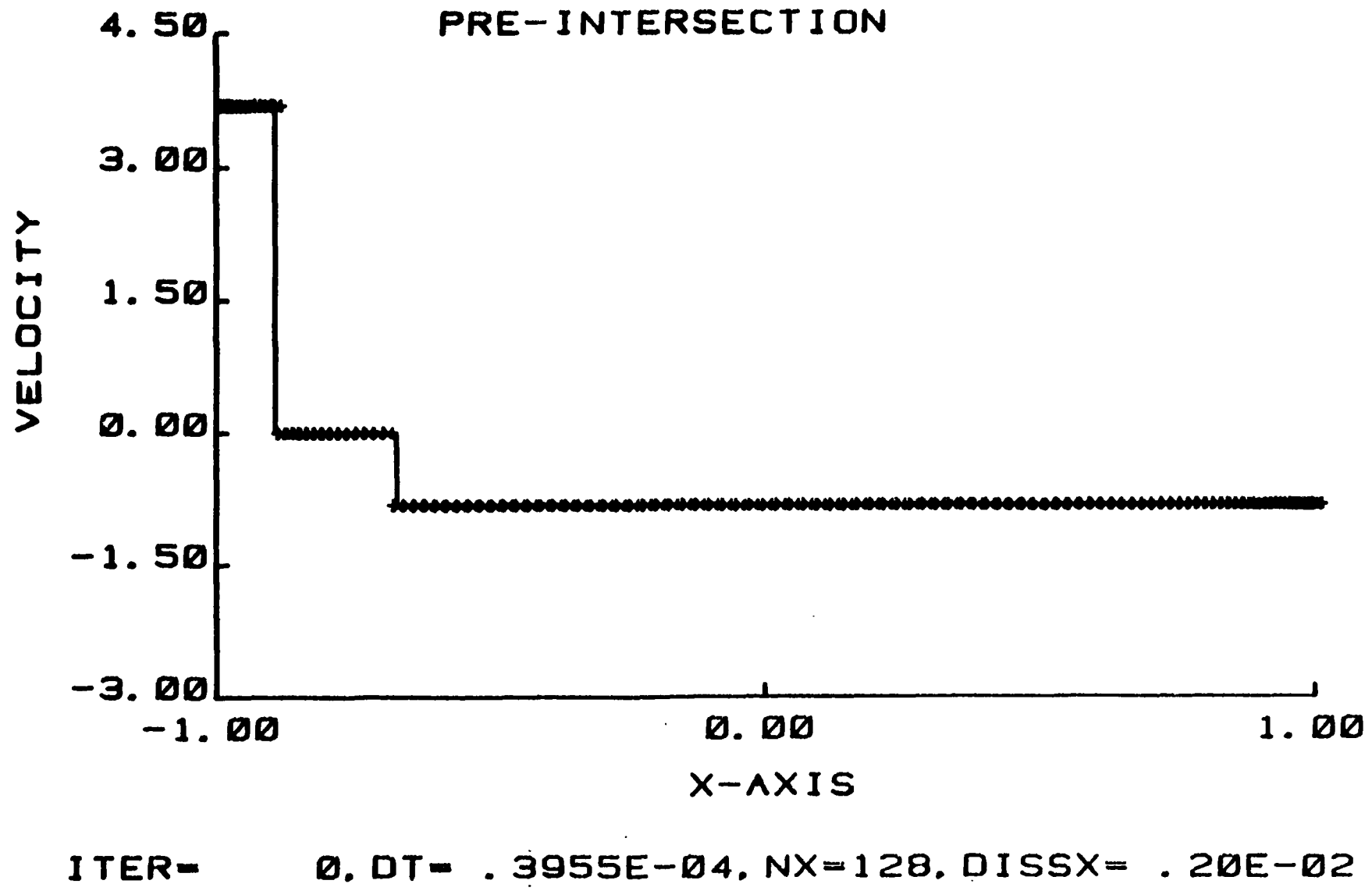

Figure 27 Colliding Shock Waves; Initial Velocity Field, Case 2.

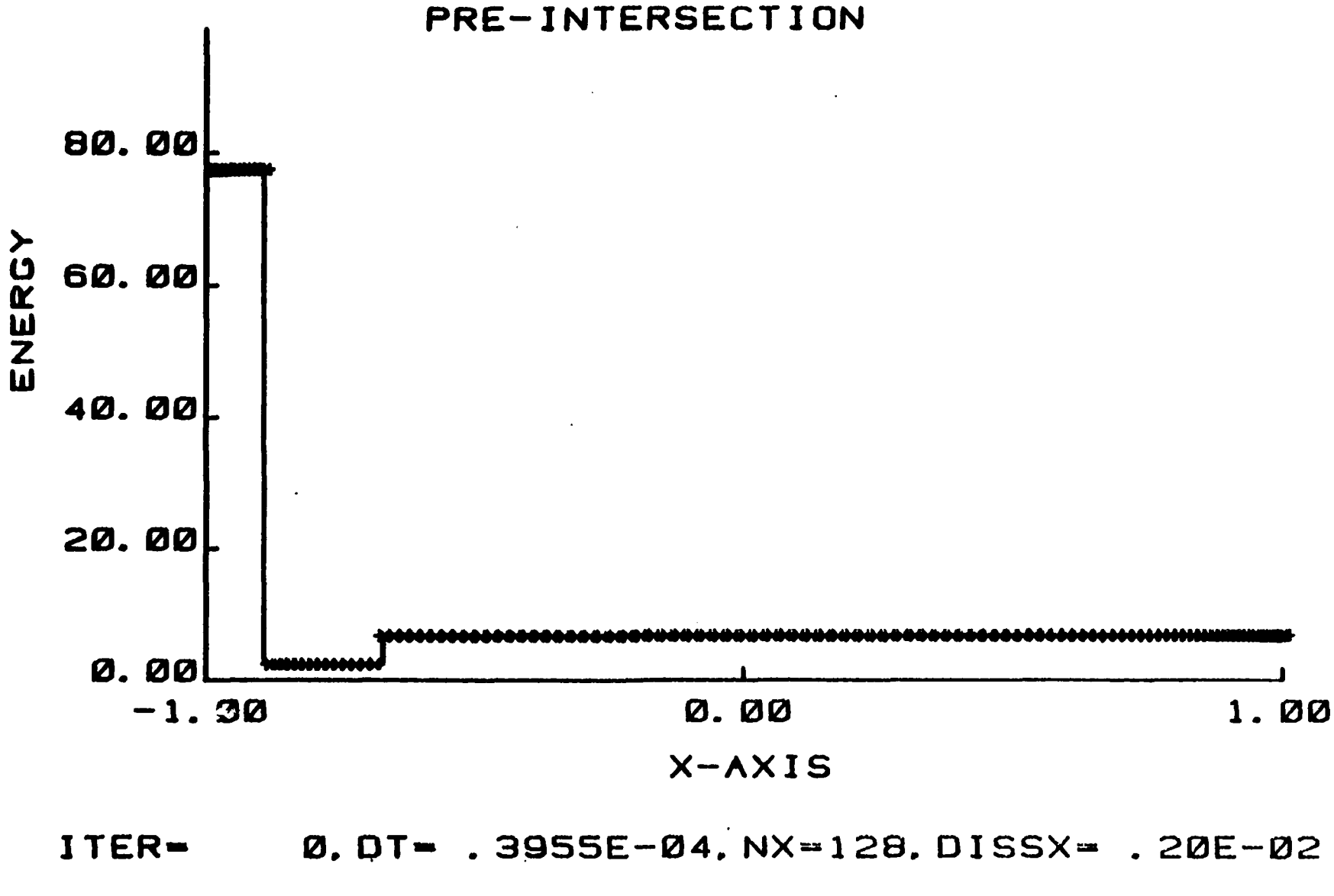

Figure 28 Colliding Shock Waves; Initial Energy Field, Case 2.

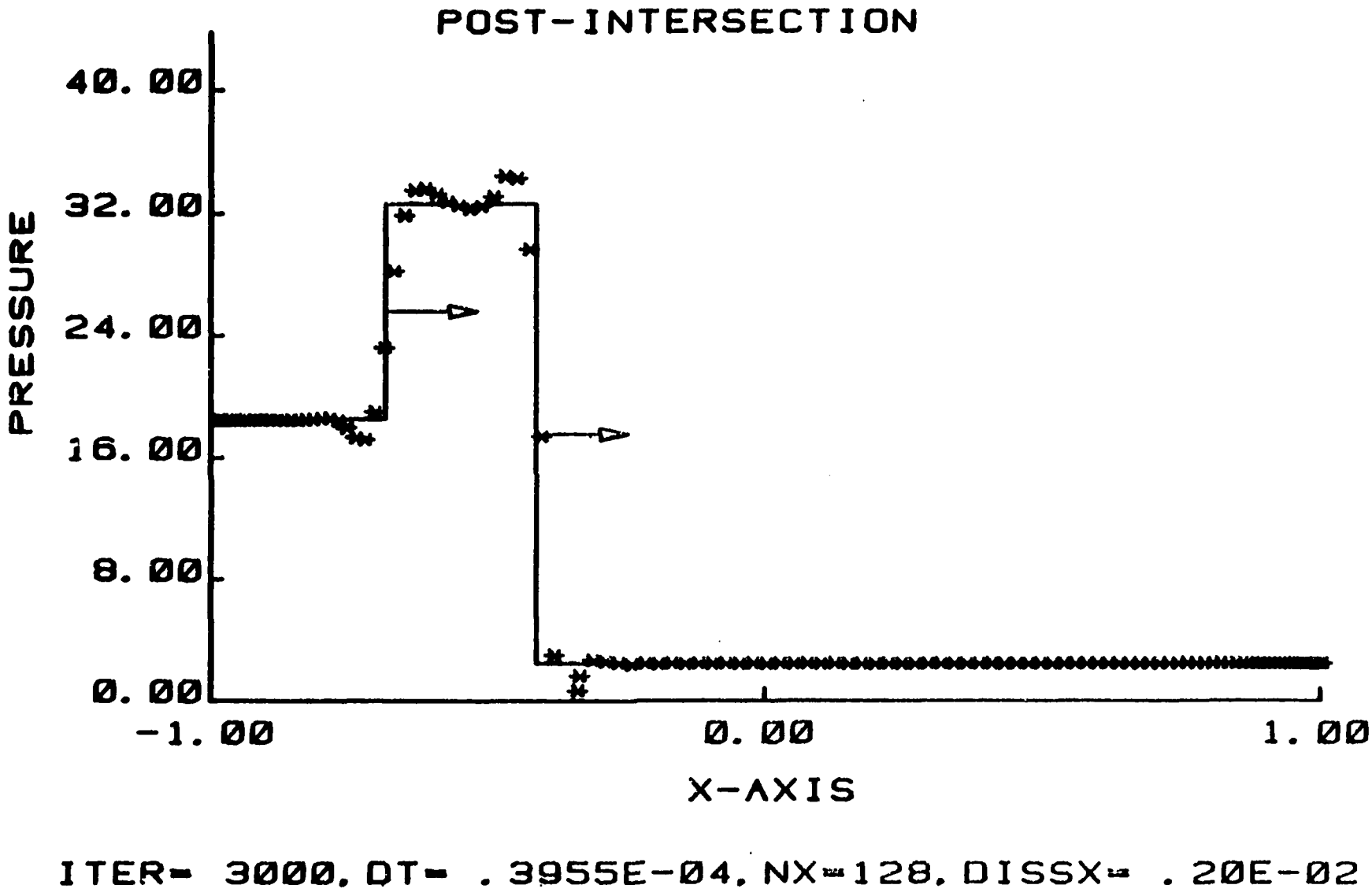

Figure 29 Colliding Shock Waves; Post-Collision Pressure Field, Case 2.

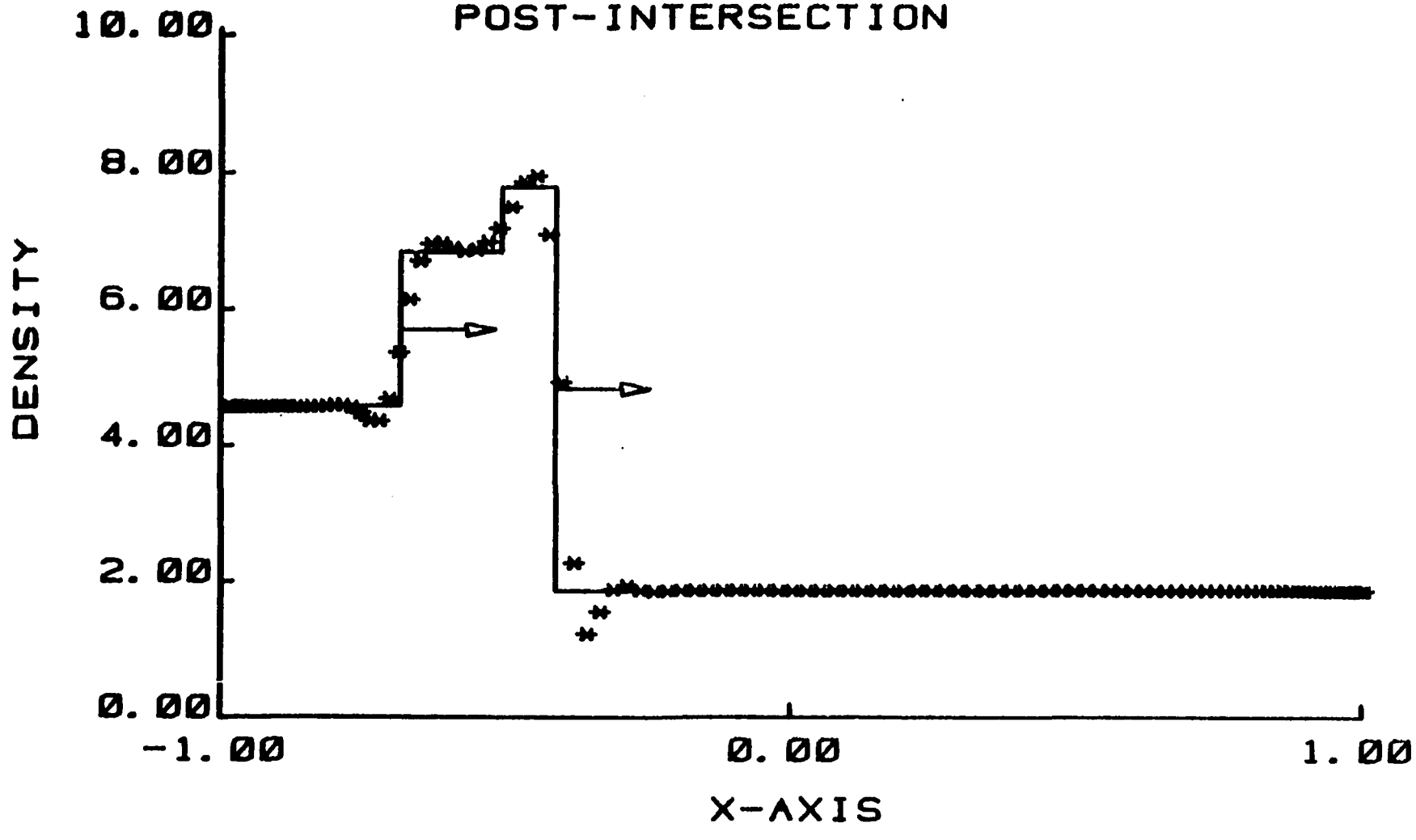

Figure 30 Colliding Shock Waves; Post-Collision Density Field, Case 2.

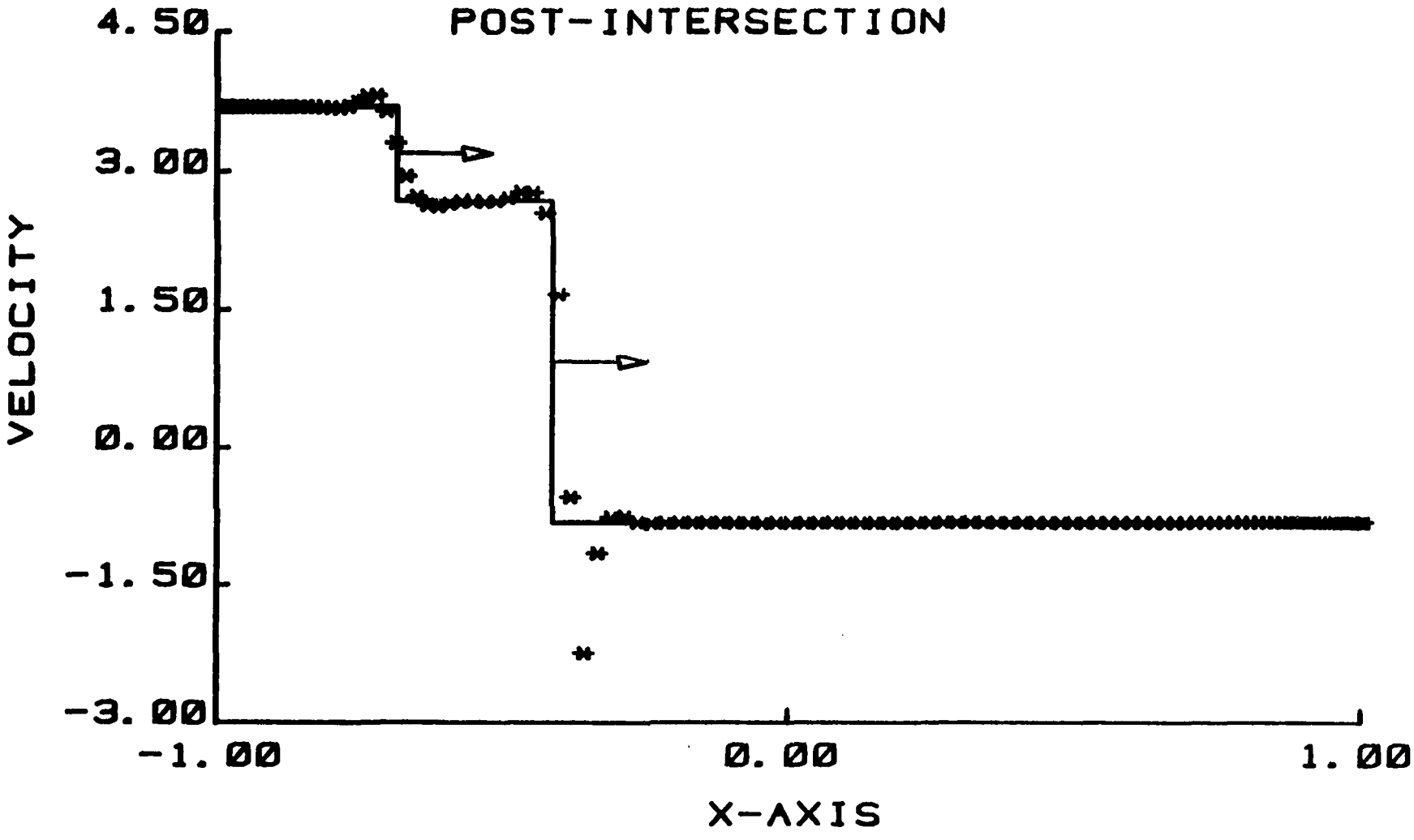

Figure 31 Colliding Shock Waves; Post-Collision Velocity Field, Case 2.

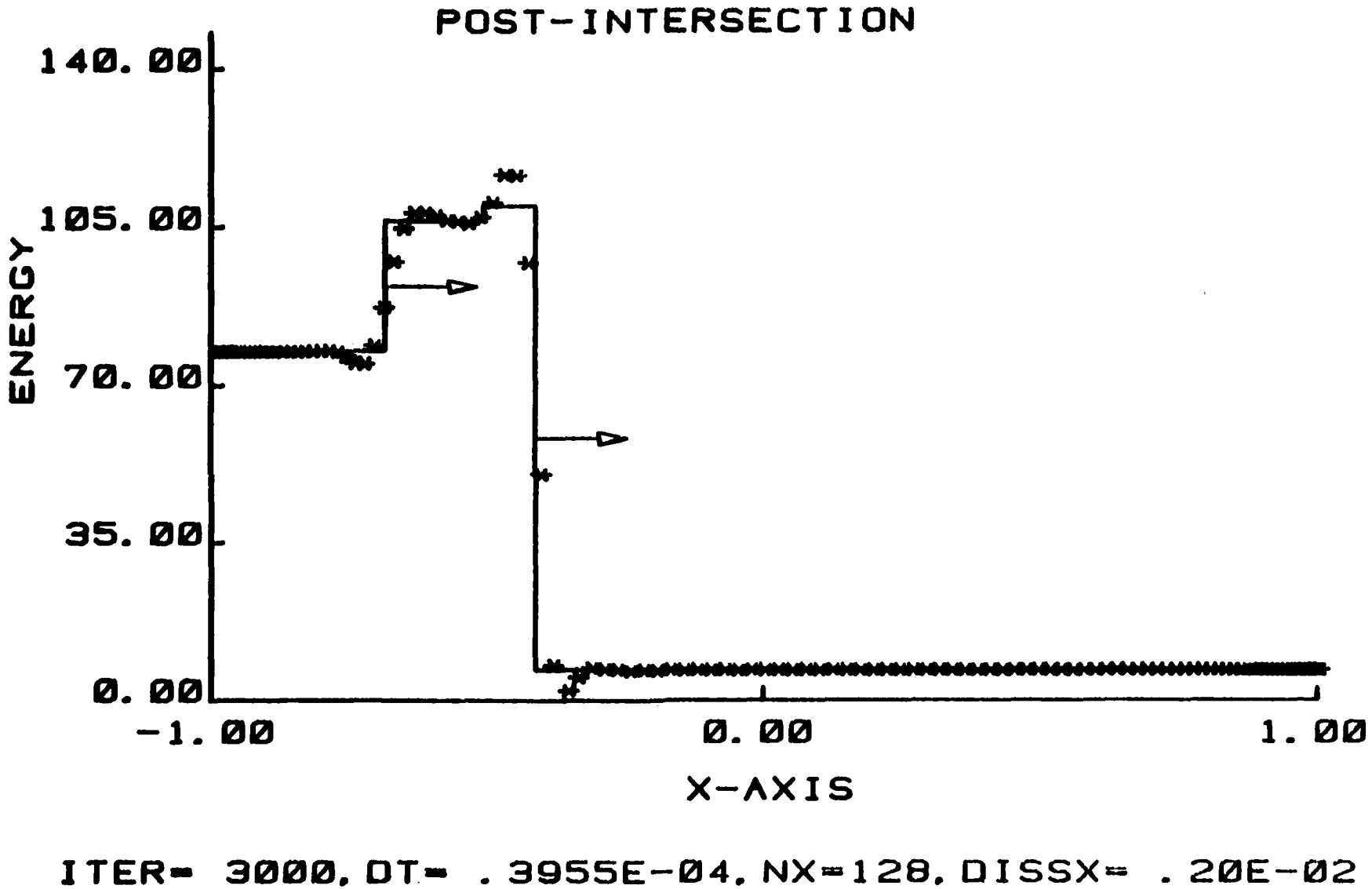

Figure 32 Colliding Shock Waves; Post-Collision Energy Field, Case 2.

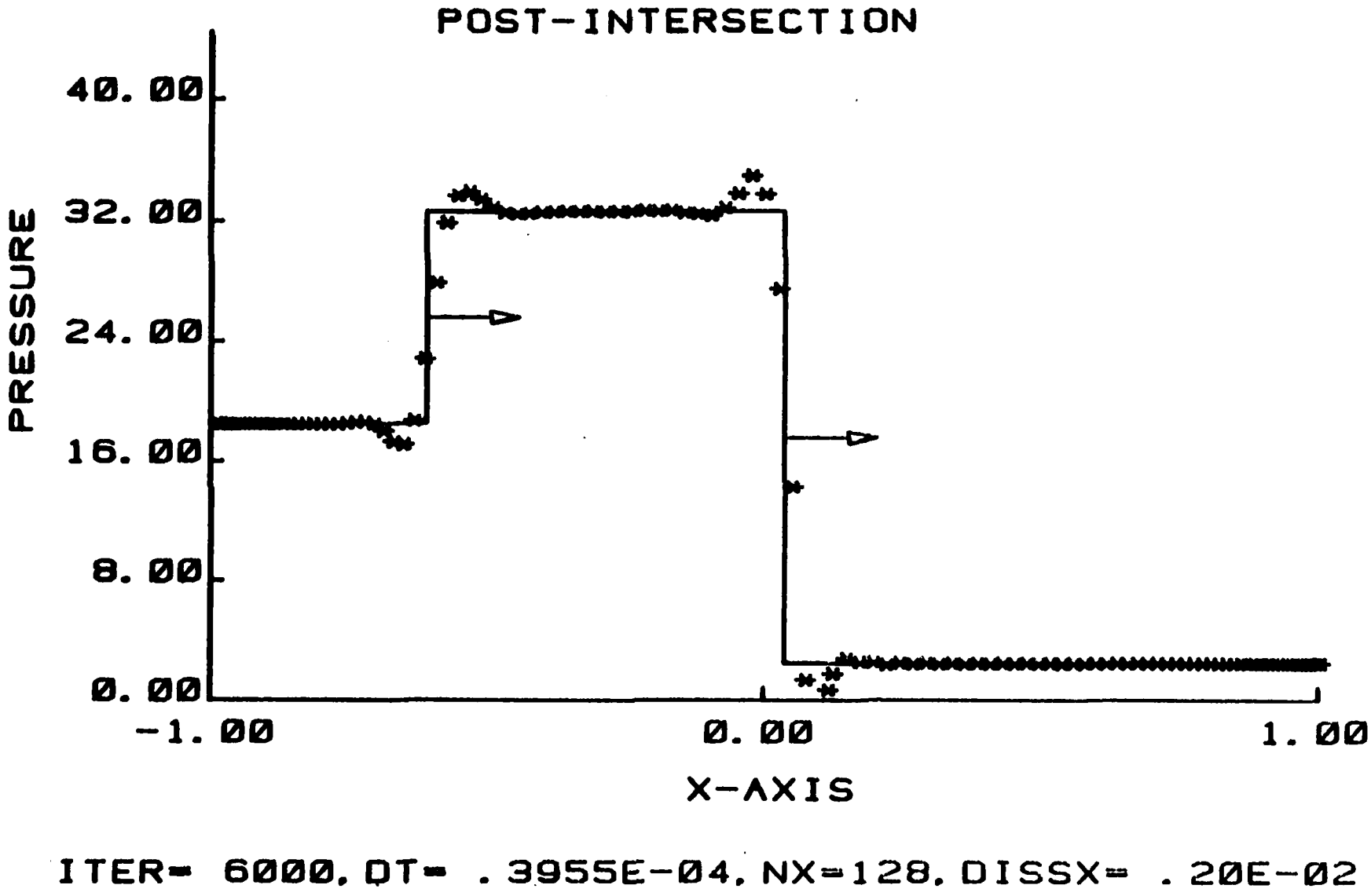

Figure 33 Colliding Shock Waves; Post-Collision Pressure Field, Case 2.

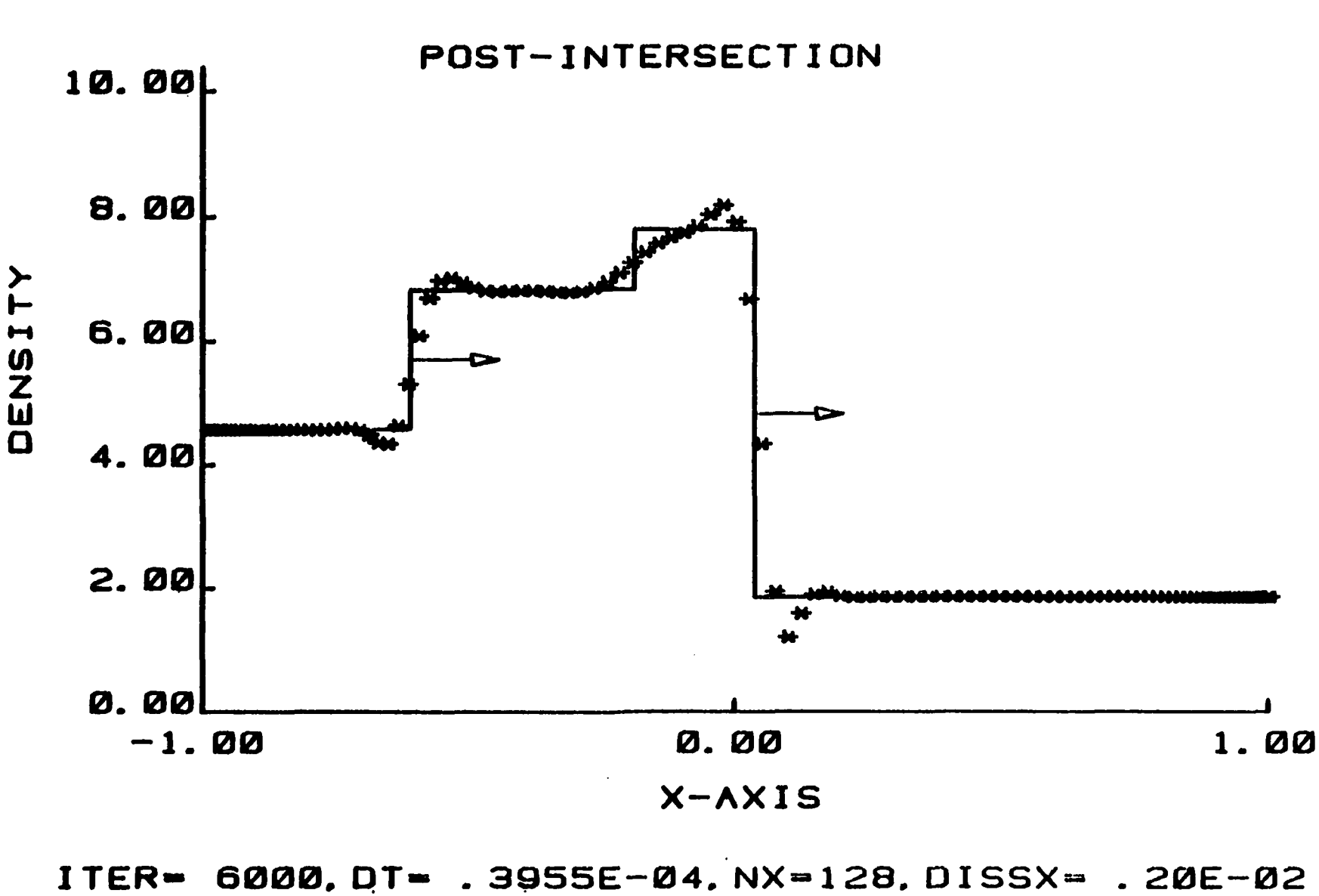

Figure 34 Colliding Shock Waves; Post-Collision Density Field, Case 2.

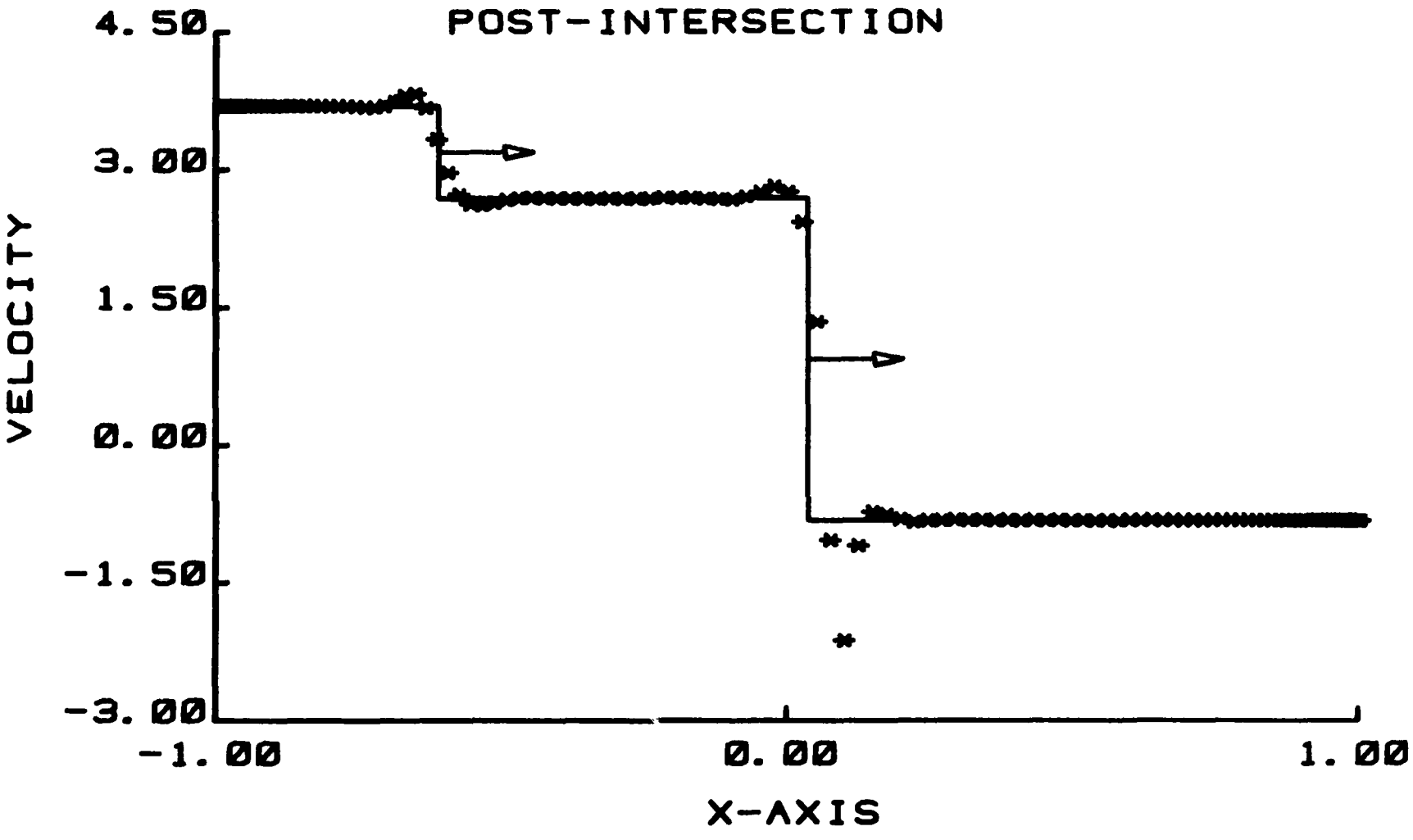

Figure 35 Colliding Shock Waves; Post-Collision Velocity Field, Case 2.

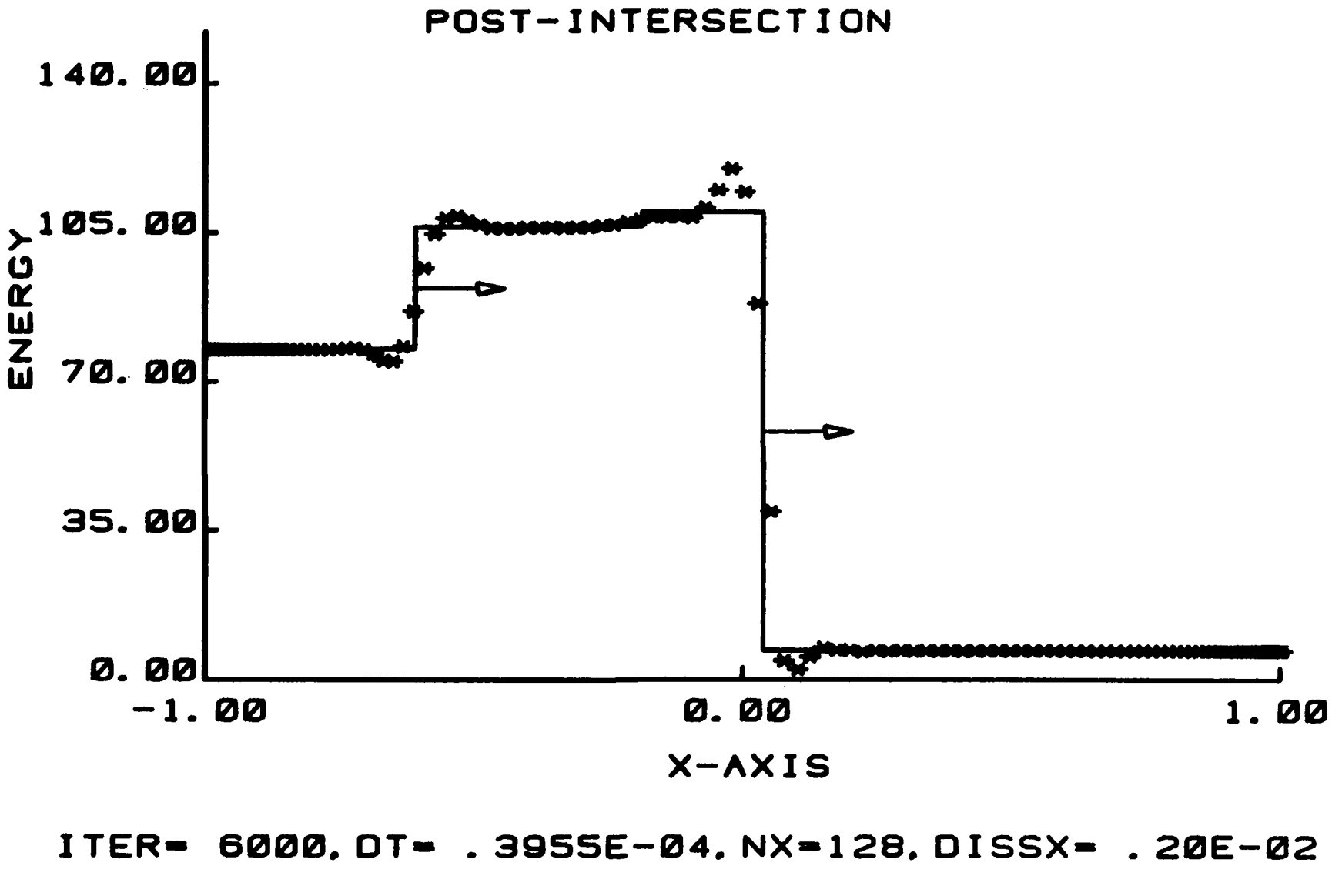

Figure 36 Colliding Shock Waves; Post-Collision Energy Field, Case 2.

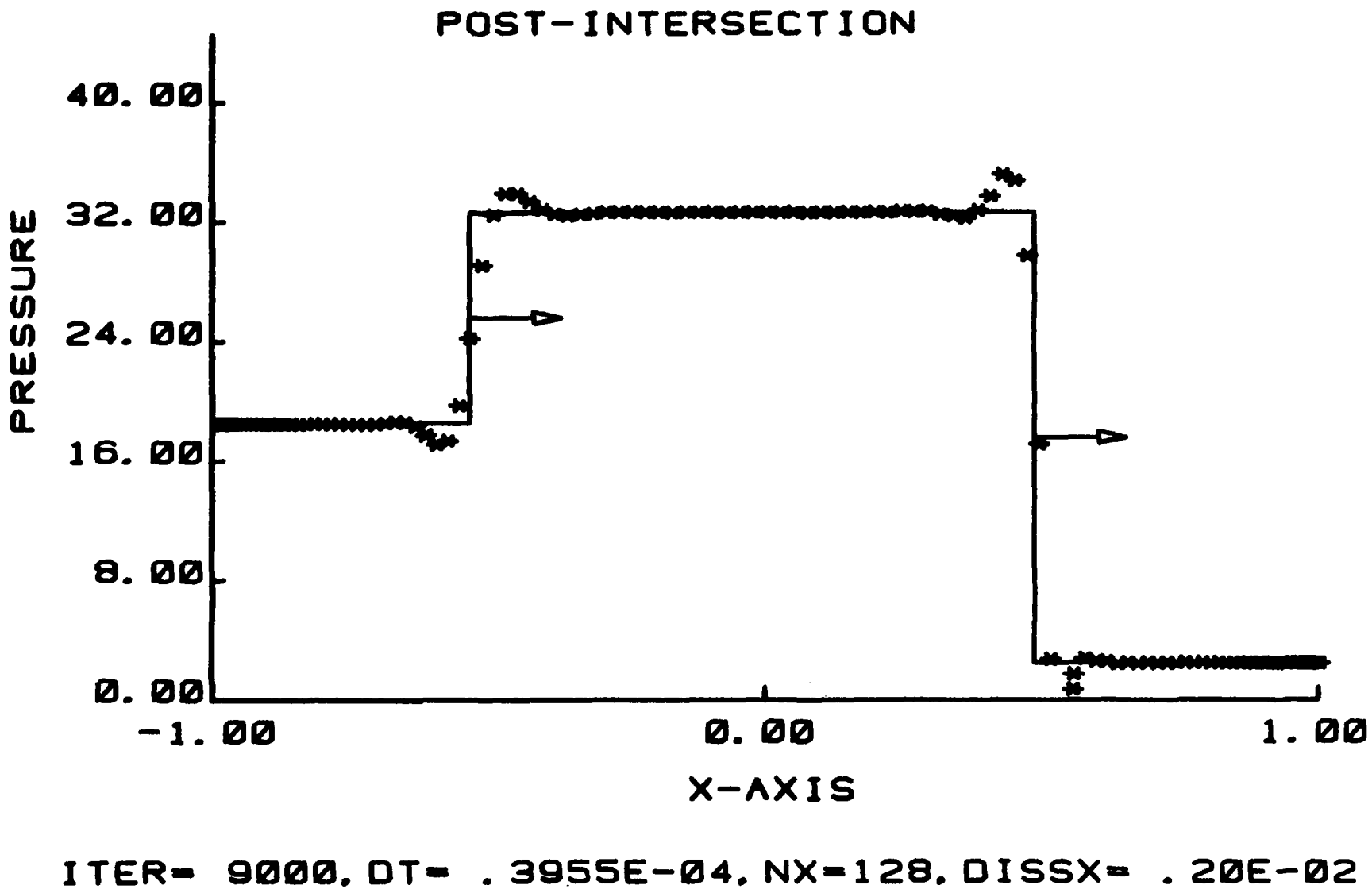

Figure 37 Colliding Shock Waves; Post-Collision Pressure Field, Case 2.

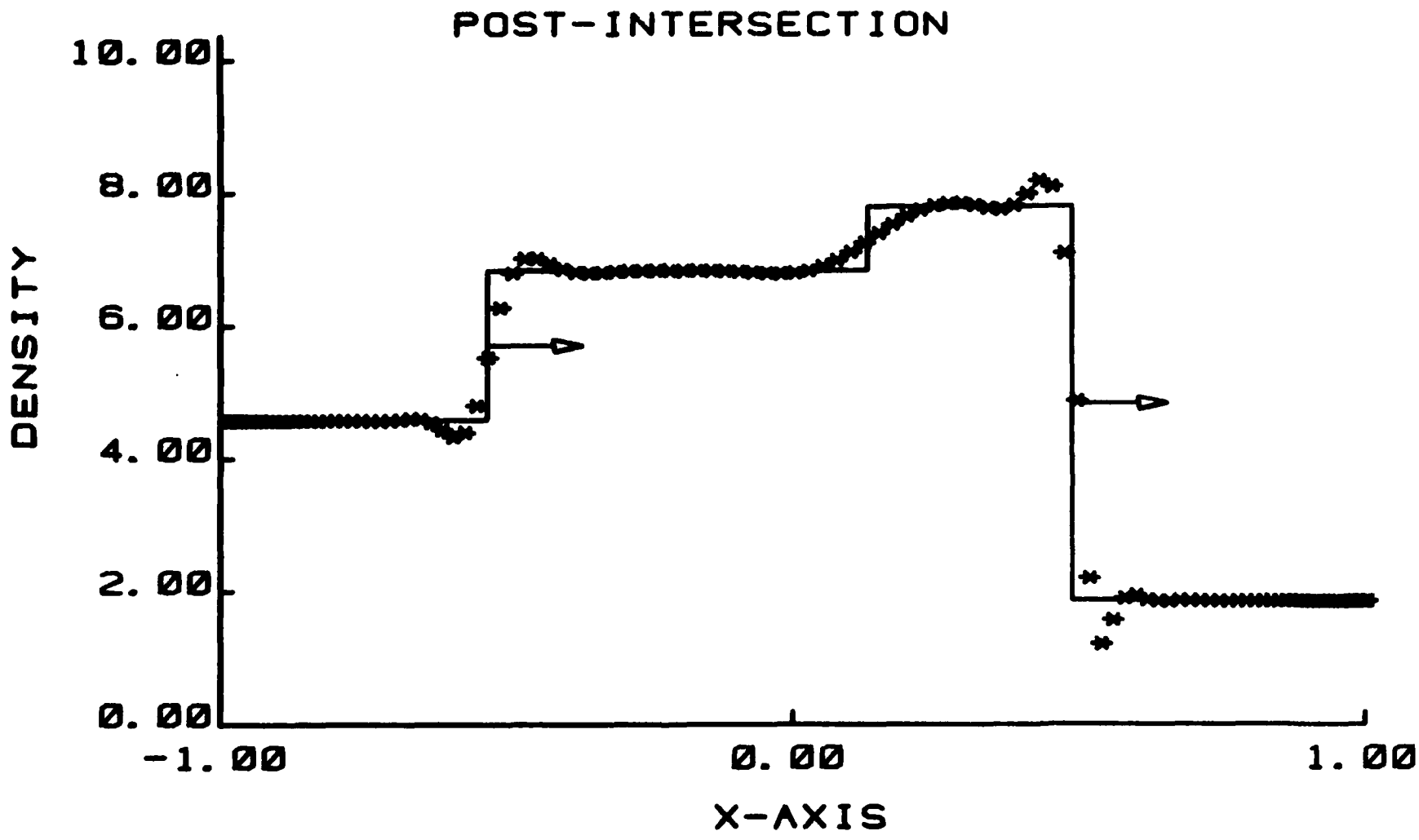

Figure 38 Colliding Shock Waves; Post-Collision Density Field, Case 2.

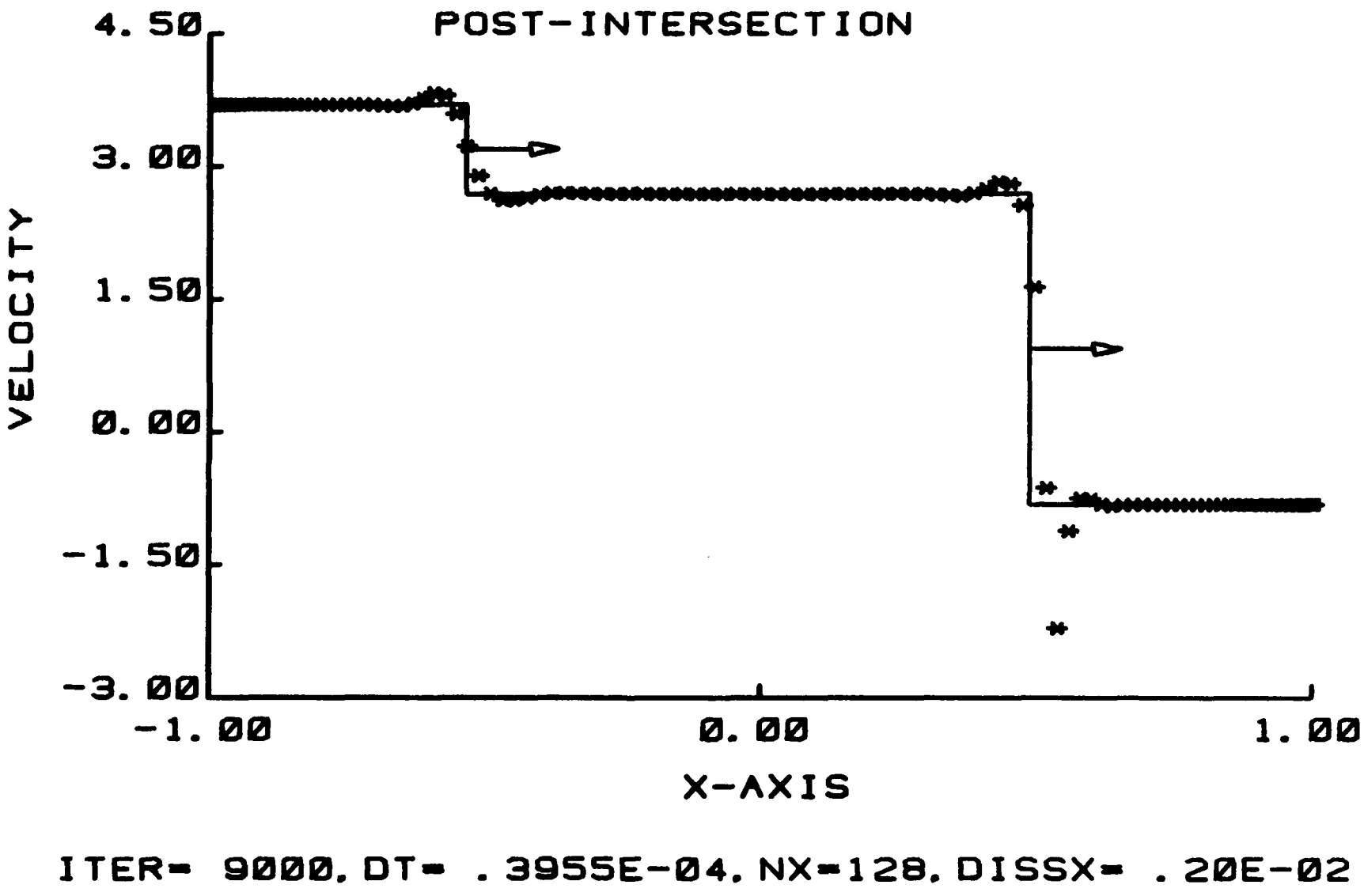

Figure 39 Colliding Shock Waves; Post-Collision Velocity Field, Case 2.

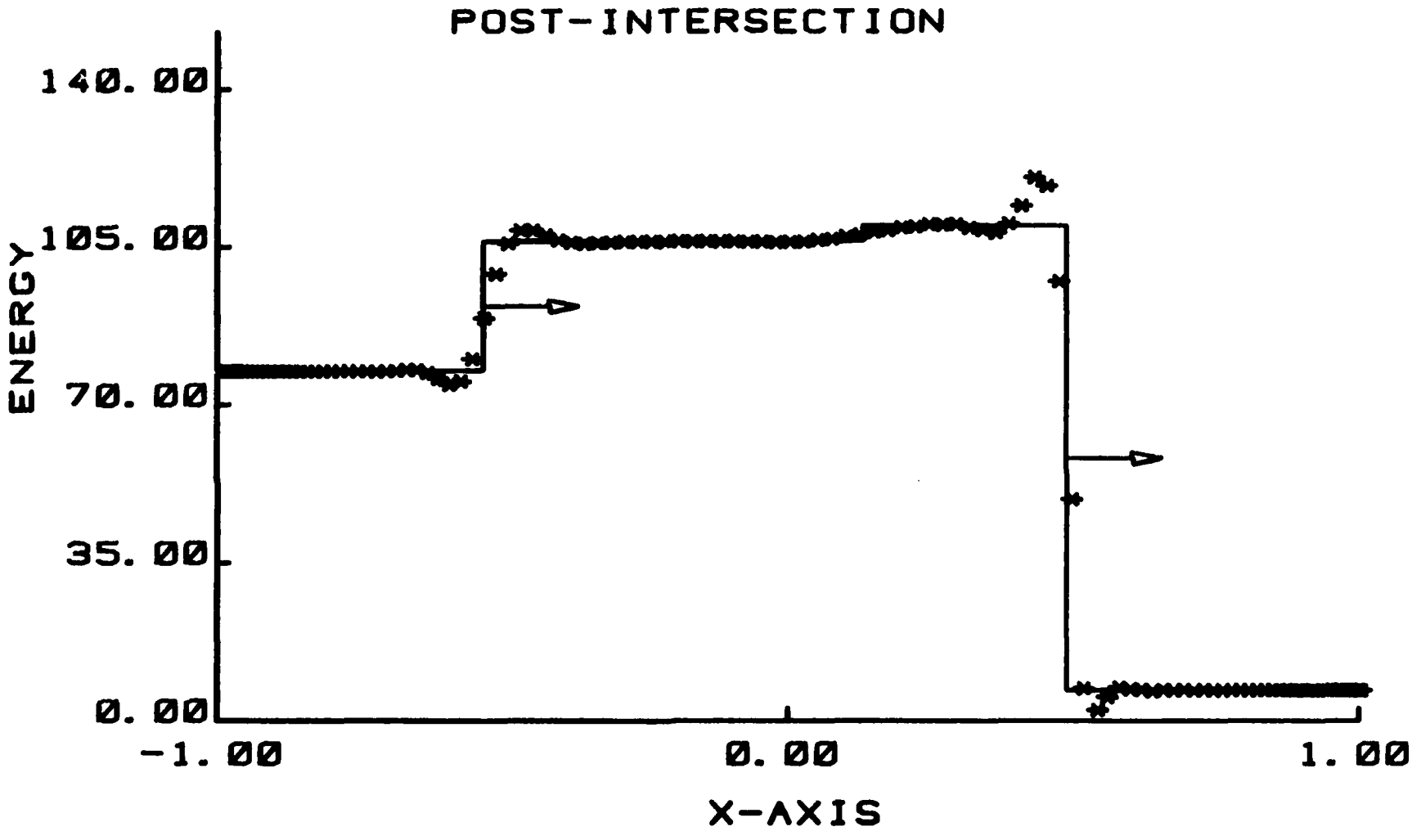

Figure 40 Colliding Shock Waves; Post-Collision Energy Field, Case 2.

VI. REFERENCES

1. Sakell, L., "Pseudospectral Solution of One-Dimensional and Two-Dimensional Inviscid Flows with Shock Waves", NRL Memorandum Report 4892, August 6, 1982.

2. Sakell, L., "Solution to the Euler Equation of Motion by Pseudospectral Techniques", paper presented at the 10th IMACS World Congress on System Simulation and Scientific Computations, Montreal, Canada, August, 1982.

3. Sakell, L., "Chebyshev-Series Solutions to the 1-D and 2-D Euler Equation With Shock Waves", paper presented at the Symposium on Spectral Methods for Partial Differential Equations, ICASE, NASA Langley, August, 1982.

4. Gottlieb, D., Lustman, L. and Orszag, S., "Spectral Calculations of One-Dimensional Inviscid Compressible Flows", SIAM J. Vol 2, No 3, September, 1981.

5. Gottlieb, D. Gunzburger, M. and Turkel, E., "On Numerical Boundary Treatment of Hyperbolic Systems for Finite Difference and Finite Element Methods", SIAM J. Vol. 19, No. 4, August, 1982.